Investigating Cognitive Load in Cyclists while Navigating in Traffic through fNIRS

Fenja Heine

Master Thesis

Human Factors and Engineering Psychology

Faculty of Behavioral, Management and Social Sciences (BMS)

University of Twente, Enschede

Supervisors

1st Supervisor: Dr. Funda Yildirim

2nd Supervisor: Dr. ir. Baran Ulak

Date: 23/06/2024

Abstract

This study aimed to understand the patterns of cognitive load in cyclists across various events by examining when and how changes in activity patterns occur during cycling, identifying which route features coincide with changes in cognitive load, and exploring how connectivity within the prefrontal cortex (PFC) is affected by different traffic conditions. Using functional near-infrared spectroscopy (fNIRS), we monitored haemoglobin oxygenation (HbO) levels in 15 participants as they navigated eight different traffic events. Our statistical analysis revealed significant increases in cognitive load in response to three events: passing over a crosswalk, passing by a pedestrian, and avoiding an object in one's path. Dynamic route features, particularly those involving interactions with pedestrians and obstacles, had a greater impact on cognitive load than static features. Connectivity analysis revealed weak to medium connections within the PFC and varying network sizes across different events, with notable differences in connectivity patterns between the right and left dorsolateral PFC (DLPFC). This indicates that some events involve more brain regions activated together, while others involve more specialized networks with fewer activated areas. Interestingly, we observed a unique patter in the left-DLPFC during the Pedestrian event, where cognitive load decreased, contrary to the increased load in the right-DLPFC. Potential factors influencing these findings include the participants' age and familiarity with the cycling route. Our findings suggest that cognitive load in cyclists is significantly affected by dynamic route features, emphasizing the need for infrastructure designs that minimize such interactions. Further research should explore these cognitive load patterns across different age groups and with more precise brain region mapping.

Investigating Cognitive Load in Cyclists while Navigating in Traffic through fNIRS

Cycling is a widely practiced mode of transportation found globally, with varying levels of accessibility and infrastructure support in different places (Horton et al., 2016). Cyclists tend to prefer routes and cities with cycling-friendly infrastructure, with notable examples including Beijing (China), Ferrara (Italy), and Oxford (UK) (Horton et al., 2016). In some cities in the Netherlands, cycling culture is well-established, with approximately half of urban journeys made by bicycle (Horton et al., 2016). While some cities have dedicated cycling paths, many cyclists share the road with motorized traffic. Cycling is increasingly appealing due to its cost-effectiveness, environmental benefits, and positive health impacts, leading countries like Germany to expand their cycling networks ("Cycling Safety," 2012b). Some initiatives taken by cities to make cycling smarter include offering cycling training for children, developing public bike hire schemes, and introducing cycle-based tourism (Fraser and Lock, 2010; Adam et al., 2018). Other ideas include giving 'open streets' events, where some roads are closed temporarily for motorized traffic for safe use for cyclists (Adam et al., 2018). In general, a lot of cities try to segregate cyclists from motor traffic by making dedicated cycling routes, or to necessitate low speed of motor vehicles in shared streets (Adam et al., 2018).

Providing safety is an important concern when working towards a well-functioning transport system, since accidents still remain a significant public health concern. Cycling itself is seen as a rather benign activity, but it is being done in a dangerous environment ("Cycling Safety", 2012b). Motorists are a primary cause of accidents and can lead to severe injuries for cyclists ("Cycling Safety", 2012b). A study by Juhra et al. (2012) found that a collision with a motor vehicle is the most prevalent cause for accidents for cyclists aged between twenty and twenty-nine years old. The risk of being involved in an accident is also influenced by factors like road design and condition ("Cycling Safety", 2012b). Poor road conditions that increase the likelihood of falling or slipping, as well as road designs that raise

the risk of collisions among traffic participants, are examples of these factors ("Cycling Safety", 2012b).

As a result of factors such as participating in motorized traffic and road design and condition, increased cognitive load can contribute to road accidents (Foy et al., 2016). Cognitive load is defined as the cognitive resources required for a specific task, it represents the relation between demands of the environment, human capacities and task performance (Causse et al., 2017). Increased cognitive load can hinder perception and attention during traffic participation (Engström et al., 2017). The inherent complexity of urban roads place substantial demands on the attentional system, making cognitive load especially critical (Foy et al., 2016; Broadbent et al., 2023). Route features that elevate cognitive load are often associated with pedestrians, parked cars, and higher traffic densities (Foy and Chapman, 2018).

Previous studies primarily examined cognitive load in the context of driving, revealing increased cognitive load during activities such as overtaking maneuvers (Foy et al., 2016). Furthermore, cognitive load rises during driving on demanding urban routes with numerous junctions and pedestrians, as compared to driving on straight roads with no pedestrians (Broadbent et al., 2023). Increased cognitive load has also been linked to reduced event detection performance, as it diverts attention away from the forward scene and narrows the field of view, thereby impairing hazard detection (Engström et al., 2005; Lee et al., 2009). Drivers under cognitive load found it challenging to recall interactions with roadway elements, including other traffic participants and road-related fixtures, following a driving session (Lee et al., 2009; Reyes and Lee, 2008). For example, they would be unable to remember passing by cyclists on the road or overlook certain traffic signs (Lee et al., 2009; Reyes and Lee, 2008). Previous research also demonstrated that drivers experiencing high cognitive demand consistently exhibited delayed braking responses, which is critical factor in road safety (Reyes and Lee, 2008; Engström et al., 2005). Interestingly, increased cognitive

load has been found to enhance driving performance in lane-keeping situations (Engström et al., 2017). This highlights that the relation between cognitive load and driving performance is not straightforward (Engström et al., 2017). However, the focus of this study is not on the relation between cognitive load and performance.

Cognitive load changes observed in drivers manifest as alterations in prefrontal cortex activity, a brain region associated with cognitive load (Foy et al., 2016). Brain activity increases with difficulty in the prefrontal cortex, but also in the cingulate gyrus, temporal and parietal regions, and insula areas on both sides (Arsalidou et al., 2013). Similarly, activity in the right thalamus increases linearly with task difficulty (Arsalidou et al., 2013). Conversely, areas such as the medial prefrontal cortex, posterior cingulate, and superior temporal gyri show decreased activity as cognitive load increases (Arsalidou et al., 2013). It is worth noting that cognitive load in adults appears to involve multiple brain regions (Arsalidou et al., 2013).

Figure 1

Overview of Brain Areas

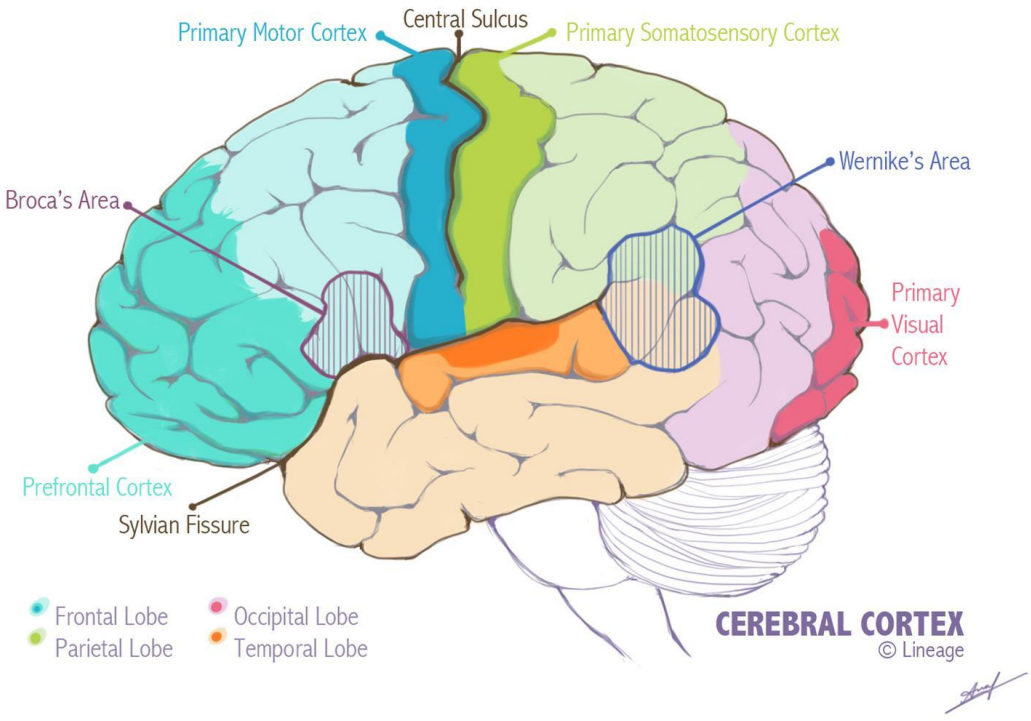

Note. Overview of different brain regions from Dominguez (2019).

Multiple brain regions are also activated together as a network when cognitive load increases, which is called functional connectivity (Liu et al., 2017). Examining functional connectivity during cognitive processes like cognitive load provides insights into how the brain's networks reorganize to handle increased demands (Bastos & Schoffelen, 2016). Research shows that the brain adapts its network organization with increasing cognitive load, particularly involving the frontoparietal executive control network (FPN) (Dimitrakopoulos et al., 2023; Zuo et al., 2019). Analyzing these connectivity patterns not only reveals engagement during tasks but also predicts performance under cognitive load, as a more responsive network is linked to better outcomes (Zuo et al., 2019; Zanto & Gazzaley, 2013; Nagel et al., 2011). An important brain area that is involved in the FPN network is the dorsolateral prefrontal cortex (DLPFC), which is part of the prefrontal cortex (PFC) (Fishburn et al., 2014). Outside of this network, it was also found that connectivity between areas within the PFC as well as between the PFC and the parietal cortex increased with cognitive load (Honey et al., 2002; Zanto & Gazzaley, 2013). When applied to driving, connections between the PFC, motor-related areas, the parietal cortex, vision-related areas, the thalamus as well as the cerebellum can be found, indicating the involvement of various brain regions in cognitive load and driving (Liu et al., 2017).

There are numerous neuroimaging methods that are suitable to detect changes in cognitive workload, such as electroencephalography (EEG) and functional magnetic resonance imaging (fMRI) (Causse et al., 2017). However, in ecological contexts, functional near-infrared spectroscopy (fNIRS) has demonstrated greater suitability for measuring cognitive load when compared to EEG and fMRI (Causse et al., 2017). fNIRS is a functional neuroimaging technique that measures changes in brain activation through the concentration of oxygenated and deoxygenated hemoglobin in the blood (Foy et al., 2016). The portability

and low motion artefact sensitivity of fNIRS sensors, as demonstrated in prior studies, make it ideal for investigating the cognitive load in naturalistic settings without participant constraints or data quality compromises (Broadbent et al., 2023; Fishburn et al., 2014).

Studies that explored the relationship between driving and cognitive load using fNIRS observed changes in oxygenated and deoxygenated haemoglobin levels in the prefrontal cortex with increasing cognitive load (Causse et al., 2017; Foy and Chapman, 2018). Specifically, research employing fNIRS to investigate cognitive load found that heightened cognitive demands led to oxygenation changes in the left dorsolateral prefrontal cortex and increased brain activation in both the right and left prefrontal cortex (Causse et al., 2017).

Based on previous research, we anticipate cyclists to experience increased cognitive load, as indicated by elevated HbO levels, during both static and dynamic route features. This increase is expected to be more pronounced in dynamic situations, since higher cognitive load has been found to coincide with dynamic route features involving pedestrians, parked cars, and other traffic participants such as moving vehicles and cyclists (Broadbent et al., 2023; Foy and Chapman, 2018). Furthermore, we expect to discover strong connections between various regions within the PFC while cycling during periods of cognitive load, as previous studies have shown that connectivity within the PFC increases with load (Honey et al., 2022; Zanto & Gazzaley, 2013).

Understanding the patterns of cognitive load in cyclists across various events can provide valuable insights into traffic safety and cyclist behavior, highlighting the critical role of cognitive load in potentially hazardous situations. Given the limited research on cognitive load in the context of cycling, this study aims to investigate when cyclists undergo cognitive load changes and how these changes manifest in brain activity and connectivity. fNIRS data, which is sensitive to cognitive load in the prefrontal cortex region, will be employed.

This research aims to address the following questions:

1. When and how do activity patterns fluctuate, as indicated by changes in oxygenated and deoxygenated haemoglobin levels, during cycling across various events (dynamic vs static route features)?
2. Which dynamic and static route features encountered during cycling cause the most prominent changes in cognitive load patterns?
3. How does synchronized activation between different regions of the PFC change when encountering static and dynamic route features, compared to when no event occurs?

Methods

To address our research questions, we utilized brain activity measurements recorded with an fNIRS device in conjunction with video footage captured by an action camera. This dataset was originally collected as a part of a thesis project at the University of Twente, the Netherlands, with the title "Unravelling the mind of cyclists: Exploring the potential of fNIRS in capturing subjective cycling experiences" (Chinpongsuwan, 2023). During the study, participants' blood oxygenation level dependent (BOLD) signals were monitored using fNIRS while cycling along a predefined route.

Data collection

In this data collection section, we reiterate the steps that were taken in the study by Chinpongsuwan (2023) for data collection.

Participants

The study by Chinpongsuwan (2023) involved 17 participants, consisting of 6 females and 11 males, aged between 19 and 35 years (M = 23, SD = 4.1). Participants were selected based on absence of psychoactive drug use, absence of brain-related disorders, and competence in cycling, such as being able to remove one hand from the steering while cycling. Informed consent was obtained from all participants (Chinpongsuwan, 2023).

Experimental Setup

The fNIRS data for the study by Chinpongsuwan (2023) was collected using the Artinis Brite MKII, a two-wavelength continuous wave system (Artinis Medical Systems, the Netherlands). The device captured blood oxygenation changes over the prefrontal cortex. The setup included 18 optodes, comprising 10 transmitters and 8 receivers, resulting in 27 measurement channels. The fNIRS data was recorded at a rate of 50Hz and transmitted to a laptop running OxySoft via Bluetooth. The OxySoft software (version 3.5.15.4., Artinis Medical Systems, the Netherlands) was developed by Artinis and allows real-time monitoring as well as offline recording of the measurements.

Route and Video Recording

Participants cycled a 7.5km route through diverse environments (Chinpongsuwan, 2023). A portion of the route exposed participants to motorized traffic, with cycling lanes running parallel to the road, sometimes without physical barriers. This section included frequent traffic stops, intersections, and interactions with other cyclists (Figure 3). Another segment of the route involved dedicated bicycle pathways away from the main road, leading through natural surroundings (Figure 4). Simultaneously, a GoPro HERO 9 action camera was used to record the cycling route from a forward-facing perspective (Chinpongsuwan, 2023).

Figure 2

Picture of Cycling Route

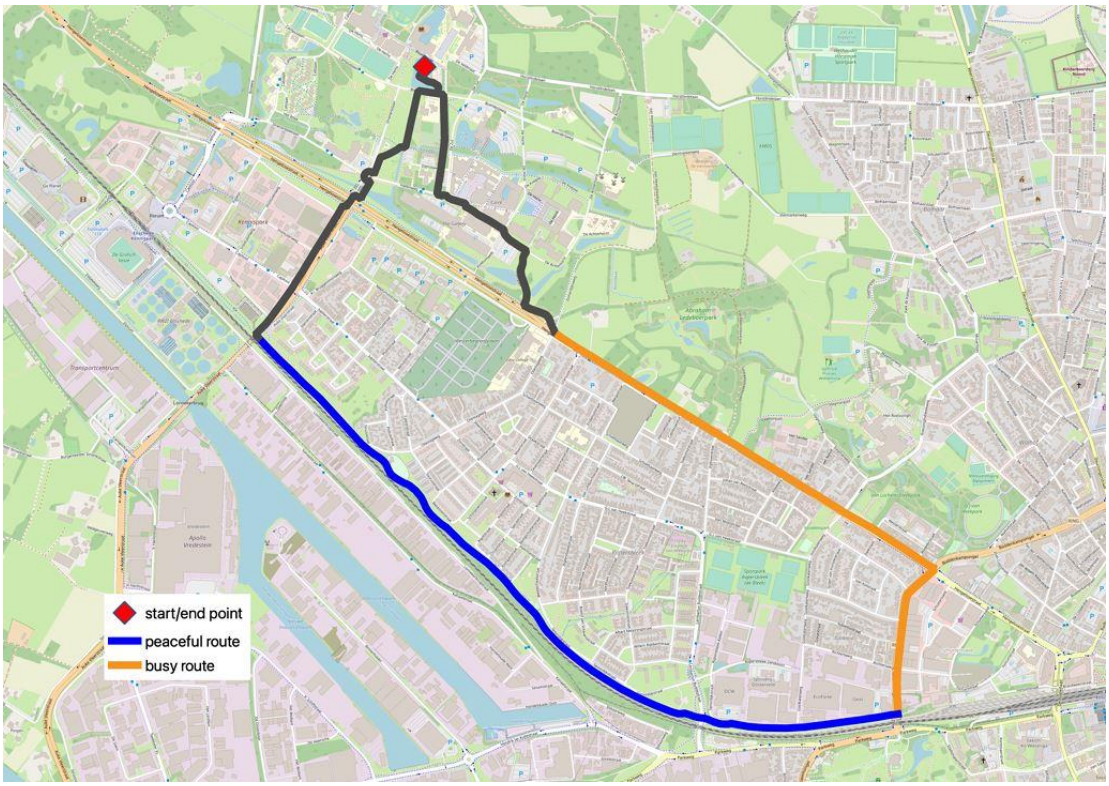

Note. This photo was taken from the thesis by Chinpongsuwan (2023). The photo shows an overview of the cycling route in Enschede, the Netherlands.

Figure 3

Picture of Motorized Traffic Route

Note. This photo was taken from the thesis by Chinpongsuwan (2023). The photo shows a part of the route through motorized traffic, located at Hengelosestraat, Enschede.

Figure 4

Picture of Bicycle Pathways

Note. This photo was taken from the thesis by Chinpongsuwan (2023). The photo shows a part of the route on a designated bicycle pathway, located at bicycle highway F35, Enschede.

Procedure and Task

For the study by Chinpongsuwan (2023), participants were instructed to abstain from alcohol and psychoactive drugs at least 24 hours before their trial, for safety reasons and to avoid potential confounding factors such as unnatural neural responses. Additionally, participants were instructed to bring their own pedal-powered bicycle; electric bicycles were not permitted for use during the trial (Chinpongsuwan, 2023). At the start of the trial, the fNIRS device was placed on the participant's head and connected via Bluetooth to a laptop running OxySoft. Optodes were carefully inspected for proper functioning, ensuring that all channels received adequate light. Subsequently, the fNIRS device was disconnected from

OxySoft in preparation for offline measurement. Participants were then escorted outside to their bicycles, where the action camera and a mobile phone (Apple iPhone XR) were mounted on their bicycle. The mobile phone was equipped with the PIEL Survey experience sampling app (pielsurvey.org), which had been preprogrammed for the experiment. After camera recording and fNIRS measurement had begun, participants were instructed to remain still for approximately two minutes to establish a baseline measurement before starting to cycle (Chinpongsuwan, 2023). Throughout the trial, the PIEL Survey app prompted participants every three minutes to rate their current feelings. Upon completion of the trial, participants engaged in a brief interview lasting approximately 10 minutes (Chinpongsuwan, 2023). During this interview, video footage captured during the ride, specifically the moments when participants received prompts form the app, was shown to the participants. They were then asked to rate their emotions during those instances. This served as a backup in case of any malfunction with the PIEL Survey app during the ride or in the event that participants failed to respond to the prompts. Additionally, participants were encouraged to provide detailed elaborations on their emotions to provide contextual information for interpreting the results (Chinpongsuwan, 2023).

Data Preprocessing

From this data preprocessing section onwards, we describe the steps we took for the present study.

The video recordings captured with the action camera were reviewed, and events observed during the participants' trials were documented. From this list of events, those that occurred frequently across multiple participants were grouped together based on similarity (e.g., the Motorized Vehicle event encompassed both cars and motorcycles), where applicable, and selected as the final event codes. Additionally, the event codes were categorized into static and dynamic road features. Static features encompassed road infrastructure elements, while dynamic features included moving elements.

Table 1

Events Classified by Static or Dynamic Route Features

Static route feature	Dynamic route feature
Traffic Light	Motorized Vehicles
Intersection	Cyclist
Roundabout	Pedestrian
Crosswalk	Avoiding Object

Note. The Avoiding Object event indicates instances where participants encountered an object blocking their path, requiring them to move around it.

The video recordings were transcribed according to these event codes. For every participant, a .xlsx sheet was generated containing columns for the start and end timestamps of each event, along with a description of the event and a brief explanation of the situation. This process was carried out for all events captured during the video recording of the trail, for all participants. Intervals during which participants cycled without encountering any road infrastructure or moving objects were labeled as Baseline.

The fNIRS data recorded during cycling sessions were converted to .snirf files (Shared Near InfraRed File Format) using OxySoft. The .snirf files were then loaded into Homer3 (Huppert et al., 2009), a MATLAB application designed to analyze fNIRS data. In Homer3, all channels were inspected for every participants and channels with poor signal quality were removed manually. Two participants were excluded from further analysis due to poor data quality or missing data.

The data were converted from intensity to optical density (OD). To remove motion artifacts, a wavelet-based motion correction was applied to the data. A low-pass filter with a cutoff frequency of 0.5 Hz was used to reduce high-frequency instrument noise and physiological noise, such as fast cardiac oscillations. This filter has been used in previous

fNIRS research (Foy et al., 2016). Subsequently, OD data were then converted to concentration data. The conversion from data to optical density and subsequently to concentration data are standard preprocessing steps for fNIRS data (Pinti et al., 2019).

The concentration data were divided into epochs, each corresponding to the timestamps of the eight events and Baseline, which were determined based on the video recordings. Following epoching, block averaging was performed over a five-second interval, spanning one second before event onset to four seconds after event onset. This five-second window was chosen because it captures the trend of the BOLD signal, which peaks between 3 and 7 seconds after stimulus onset, ensuring a comprehensive view of the hemodynamic response despite varying event durations (Yeşilyurt et al., 2008; Hillman, 2014; Wilcox & Biondi, 2015). Although the hemodynamic response begins within 1-2 seconds, observing the full response from onset to peak (2*2 seconds = 4 seconds) and accounting for event length variability makes the five-second window optimal (Wilcox & Biondi, 2015). A hemodynamic response function (HRF) model was fitted over the block averages. Fitting an HRF model is a common preprocessing step in analyzing fNIRS data, which helps to interpret the neural correlates of cognitive processes more accurately (Dans et al., 2021). The resulting HRF values were exported from Homer3 as a .txt file.

In our analyses, we focused on oxygenated hemoglobin (HbO) values, as they have demonstrated a stronger correlation with blood flow compared to deoxygenated hemoglobin, thus serving as a more reliable marker of hemodynamic activation (Fishburn et al., 2014).

HbO HRF values from channels positioned over the dorsolateral prefrontal cortex (DLPFC) were extracted from the exported .txt file and organized into a separate file. The DLPFC was chosen as the region of interest due to its frequent association with cognitive load. Previous studies have consistently linked cognitive load with HbO levels in the DLPFC (Peck et al., 2014; Unni et al., 2015; Bunce et al., 2011), with significantly higher blood oxygenation levels observed during tasks involving increased cognitive load (Bishop et al.,

2021). Each hemisphere of the DLPFC appears to be more dominant for different types of cognitive workload; for instance, the left-DLPFC is more implicated in tasks requiring memory load, while the right-DLPFC is dominant during vigilance-related tasks (Causse et al., 2017). Data from optodes positioned over both sides of the DLPFC were analyzed, as cognitive workload affects both hemispheres (Lim et al., 2020).

Each hemisphere was represented by two channels corresponding to the DLPFC. For the right-DLPFC, channels between optodes Tx2, Rx1 and Rx3 (channels 2,1 and 2,3) were analyzed. Likewise, for the left-DLPFC, channels between optodes Tx10, Rx7 and Rx8 were examined (channels 10,7 and 10,8).

Figure 5

Artinis Optode Template Guide

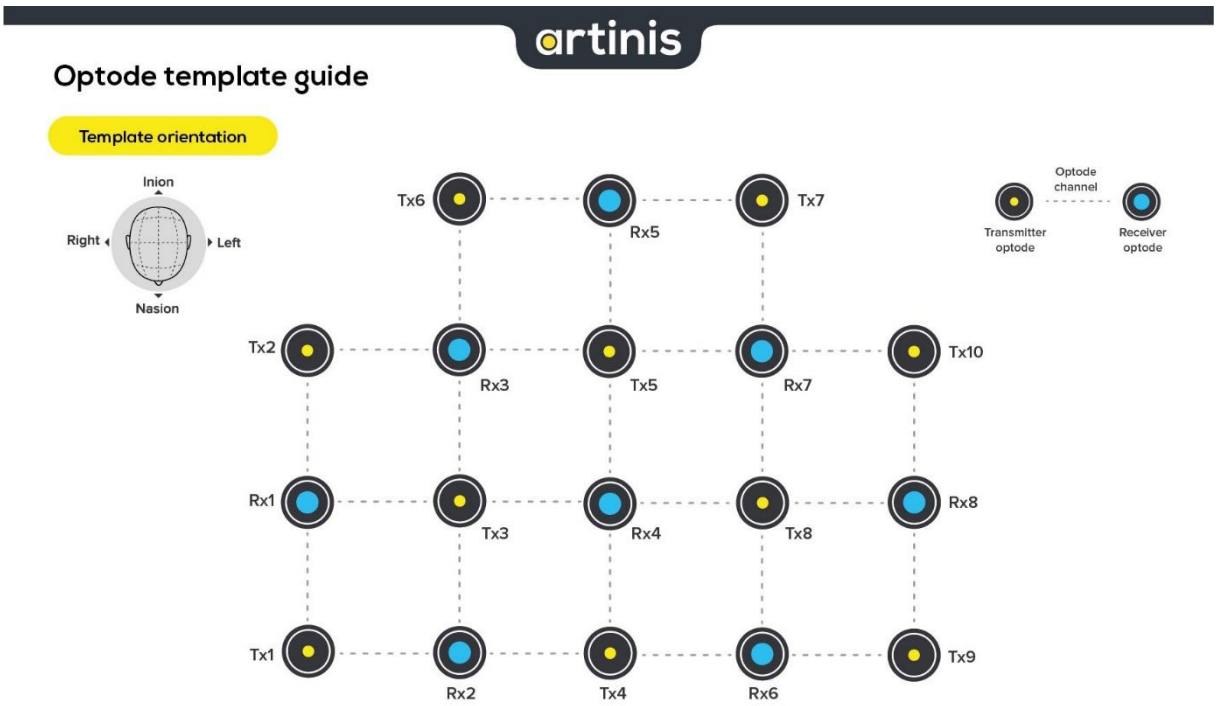

Note. This optode template guide was taken from the website of Artinis (Artinis Medical Systems, 2024).

Statistical Analysis

Statistical analyses were conducted using the R programming language within RStudio (RStudio Team, 2024). To address the first and second research question, which pertain to changes in activity patterns during cycling across various events and the relationship between route features and changes in cognitive load, t-tests were performed.

Analyses were differentiated based on hemisphere, focusing separately on the right and left-DLPFC. For each event type, t-tests were conducted for all time points of the block averages of five seconds, comparing the event's HbO HRF values to those of the Baseline. For each comparison, graphs were generated to visualize the fluctuation of HbO HRF values for both the event and Baseline. Significance thresholds were marked on the graphs to indicate moments where HbO HRF values differed significantly between the event and Baseline conditions.

Connectivity Analysis

For the connectivity analysis, the block-averaged concentration data, which are the averages of the preprocessed data, were utilized instead of the HRF-fitted data. This concentration data were obtained by accessing the .mat files generated during the preprocessing of the data in Homer3. Each participant's preprocessing result is stored in these .mat files. Subsequently, the .mat files were converted to a .txt format using MATLAB, then imported into Excel and saved as .xlsx files. The data were organized by extracting the HbO values from each participant's file for a specific event and channel, and aggregating them into new files. This resulted in a file structure comprising nine folders, each corresponding to one of the eight events and Baseline. Within each event and Baseline folder, there are 27 .xlsx files, with each file representing one channel and containing the HbO values of all 15 participants for that event and channel (i.e., each file contains 15 columns, one for each participant).

Functional connectivity is estimated by calculating the correlations between nodal activities based on BOLD signals collected during a certain task (Liu et al., 2017). For each event and Baseline, correlations between all possible channel pairs were calculated using Python (Python Software Foundation, 2021). The resulting correlation matrices were saved as .xlsx files (see Appendix). Additionally, two different plots were generated for each event and Baseline to illustrate the results of the connectivity analysis. The two plots were merged into one figure for each event and Baseline. To visualize the connectivity between the different channels, the MNI coordinates of the channels were extracted from OxySoft by digitizing the optodes and creating a topograph. The right plot in the figures shows medium or strong correlations on a topographic map, generated in Python using the NetPlotBrain package (Fanton & Thompson, 2023). The left plot in the figures was created using the Matplotlib library (Hunter, 2007), illustrating the varying strengths of correlations between channels and indicating the location of each channel within the PFC.

Results

Static Route Features: Comparison between Baseline and Events

As a result of the t-tests for the static route features, one of the four events of this category showed a significant difference in haemoglobin oxygenation levels with Baseline. The overview in Table 2 shows all results for the static route features, including the insignificant results. The blue graph lines represent Baseline, the red graph lines represent the respective event. Grey shaded areas in a figure show where a significant difference in HbO levels was found. Bigger versions of the figures for insignificant results can be found in Appendix A.

Table 2

Overview of Static Route Features Results

Right-DLPFC	Left-DLPFC

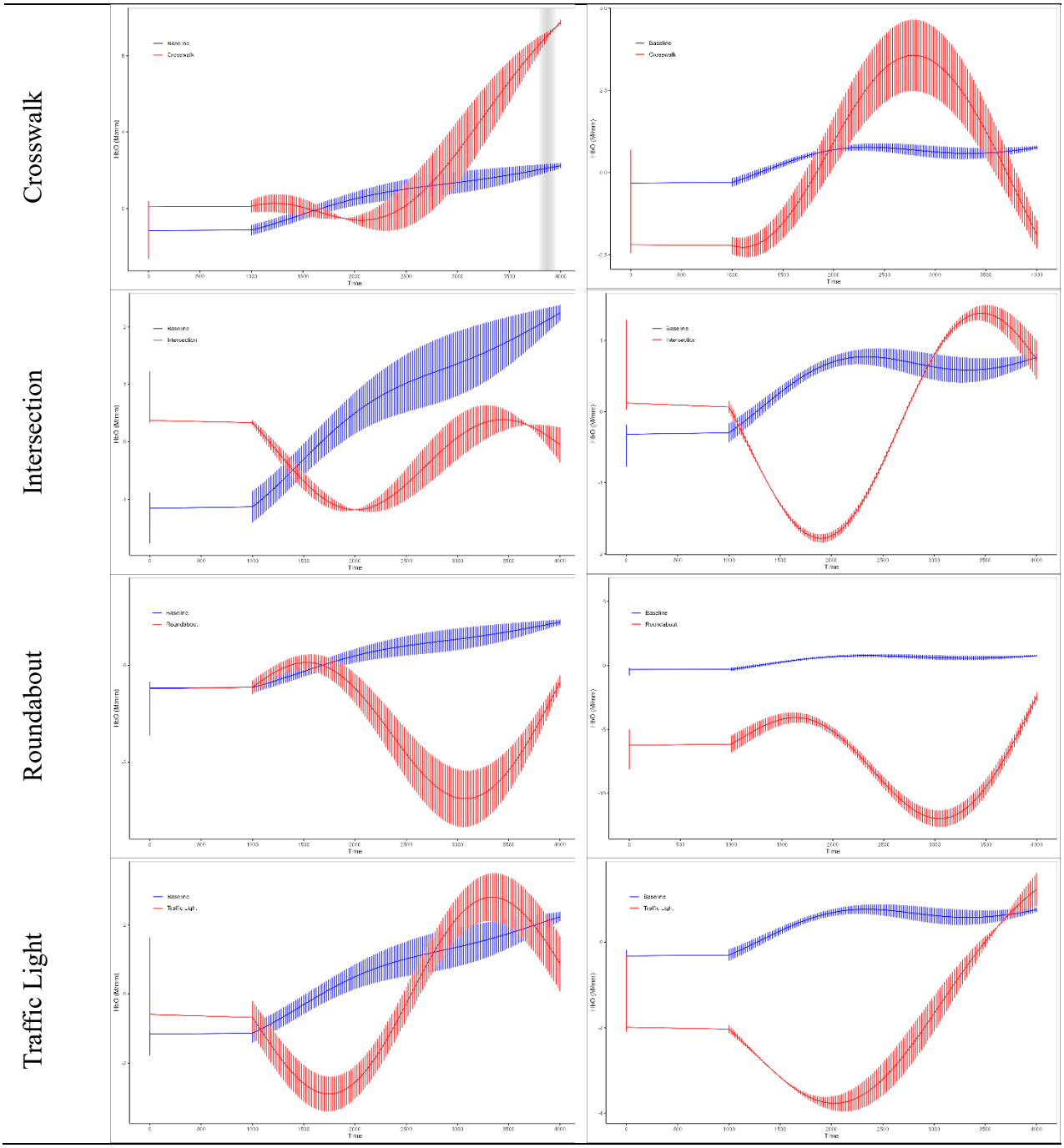

From the trend overview in Table 2, we see how the HRF HbO levels, and therefore cognitive load, during different events compared to cognitive load during Baseline, when no event happened. When the HRF HbO values for an event were higher than Baseline, it indicated more activity in either the right or left DLPFC, suggesting increased cognitive load during that event. When the HRF HbO values for an event were lower than Baseline, it

suggested lower activity and therefore decreased cognitive load during that event. A similar overview for the dynamic route features is provided in Table 4.

Static Route Features: Right-DLPFC

The comparison between the Crosswalk event and Baseline revealed a statistically significant difference ($p < 0.05$) in hemodynamic responses within the right-DLPFC between time points 3840 and 3900, as indicated by the shaded area in the graph (Figure 6). Figure 6 depicts the comparison of HbO HRF values, representing the concentration of HbO in units of Molar per millimeter (M/mm), between the Crosswalk event and Baseline.

Figure 6

Comparing Event Crosswalk with Baseline at the Right-DLPFC

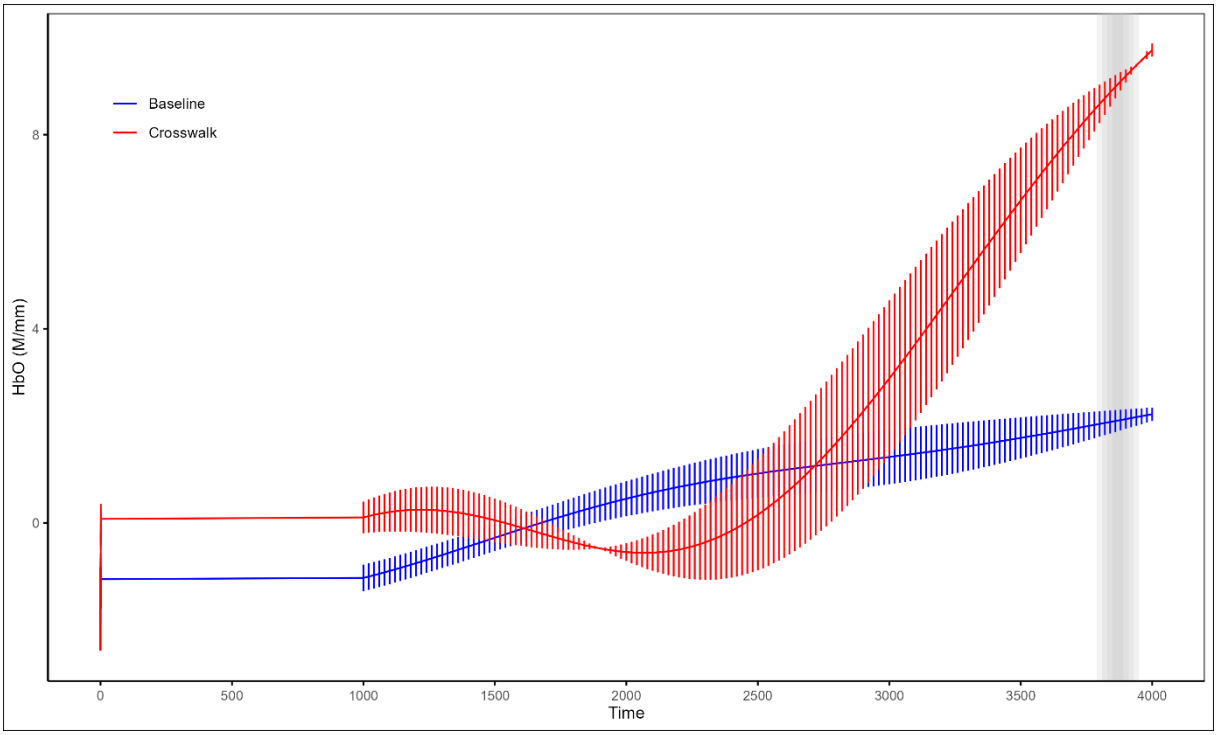

Note. The x-axis represents time in milliseconds (ms), with time point 0 indicating the onset of the event. Shaded areas represent time intervals where significant differences ($p < 0.05$) between Baseline and Crosswalk event were detected based on t-tests. Error bars indicate the standard error of the averaged signal.

The corresponding t-test results for this interval are summarized in Table 3. The table only shows the t-test results for the time points where there was a significant difference between the Crosswalk event and Baseline. During the interval where we found a significant difference, the HbO HRF values for the Crosswalk event were higher than those for Baseline. This means there was more activity, and therefore more cognitive load, in the right-DLPFC during the Crosswalk event compared to when no event was happening.

Table 3

Results from T-tests Comparing Event Crosswalk with Baseline for the Right-DLPFC

Time Point (ms)	Mean Crosswalk (M/mm)	Mean Baseline (M/mm)	t-value	p-value
3840	8,869	2,079	17,537	0,036
3860	8,985	2,099	67,500	0,009
3880	9,099	2,119	37,718	0,016
3900	9,211	2,139	14,929	0,042

For the static route features, no other significant differences in haemoglobin oxygenation levels between Baseline and any of the other events were found.

Dynamic Route Features: Comparison between Baseline and Events

The t-tests for the dynamic route features revealed significant differences in hemoglobin oxygenation levels with Baseline for two events. For the Pedestrian event, significant results were found for both sides of the DLPFC. The overview in Table 4 shows all results for the dynamic route features, including the insignificant results. The blue graph lines represent Baseline, the red graph lines represent the respective event. Grey shaded areas in a figure show where a significant difference in HbO levels was found. Bigger versions of the figures for insignificant results can be found in Appendix A.

Table 4

Overview of Dynamic Route Features Results

	Right-DLPFC	Left-DLPFC
Avoiding Object	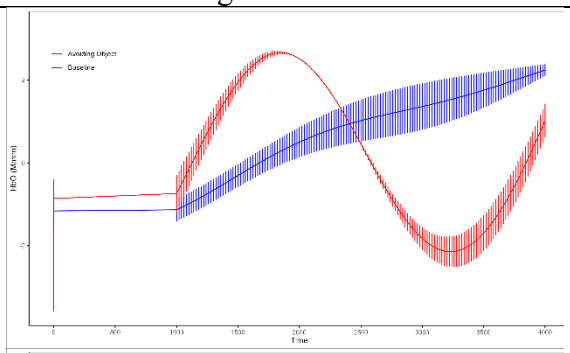	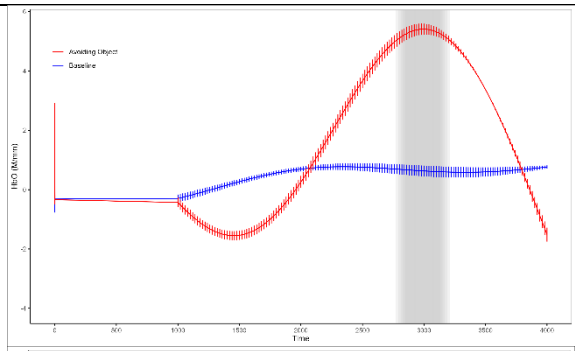
Cyclist	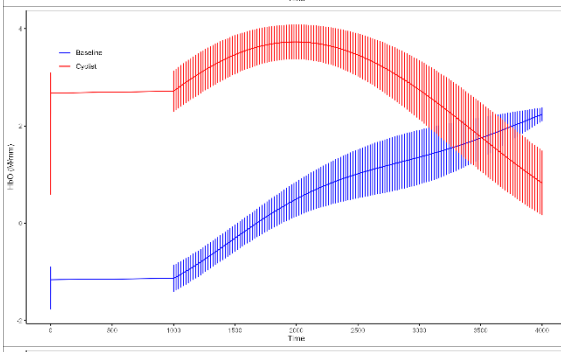	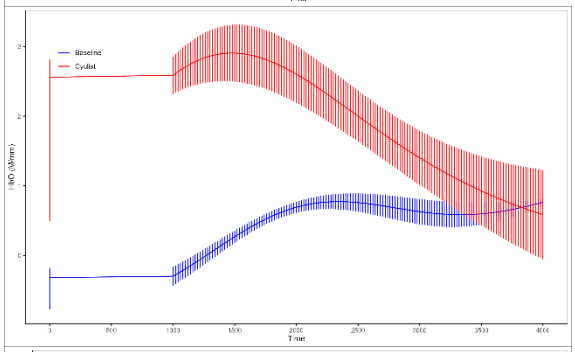
Motorized Vehicle	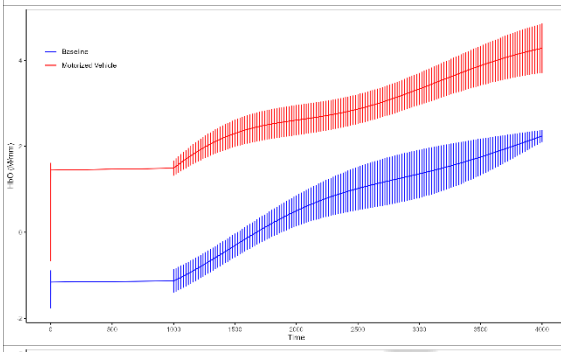	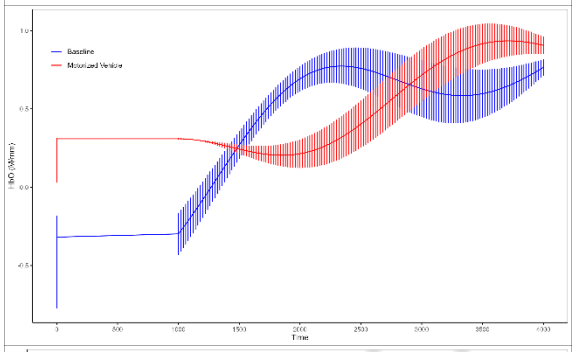
Pedestrian	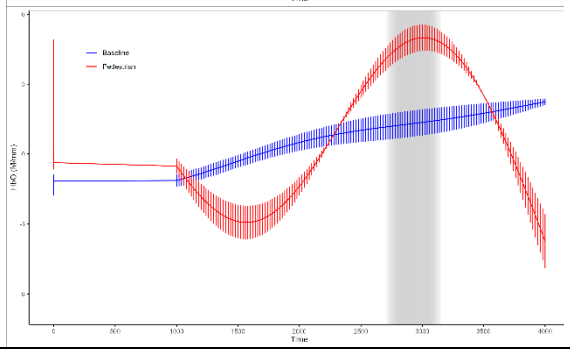	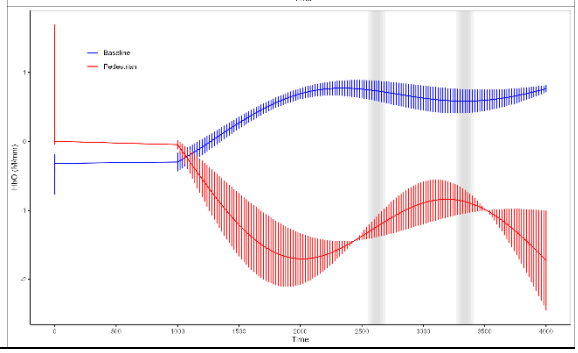

Dynamic Route Features: Right-DLPFC

During the Pedestrian event at the right-DLPFC, significant differences in hemoglobin oxygenation levels were detected compared to Baseline as well between time points 2760 and

3100. The HbO HRF means in M/mm for Baseline and Pedestrian that differed significantly ($p < 0.05$) are indicated by the shaded area in Figure 7.

Figure 7

Comparing Event Pedestrian with Baseline at the Right-DLPFC

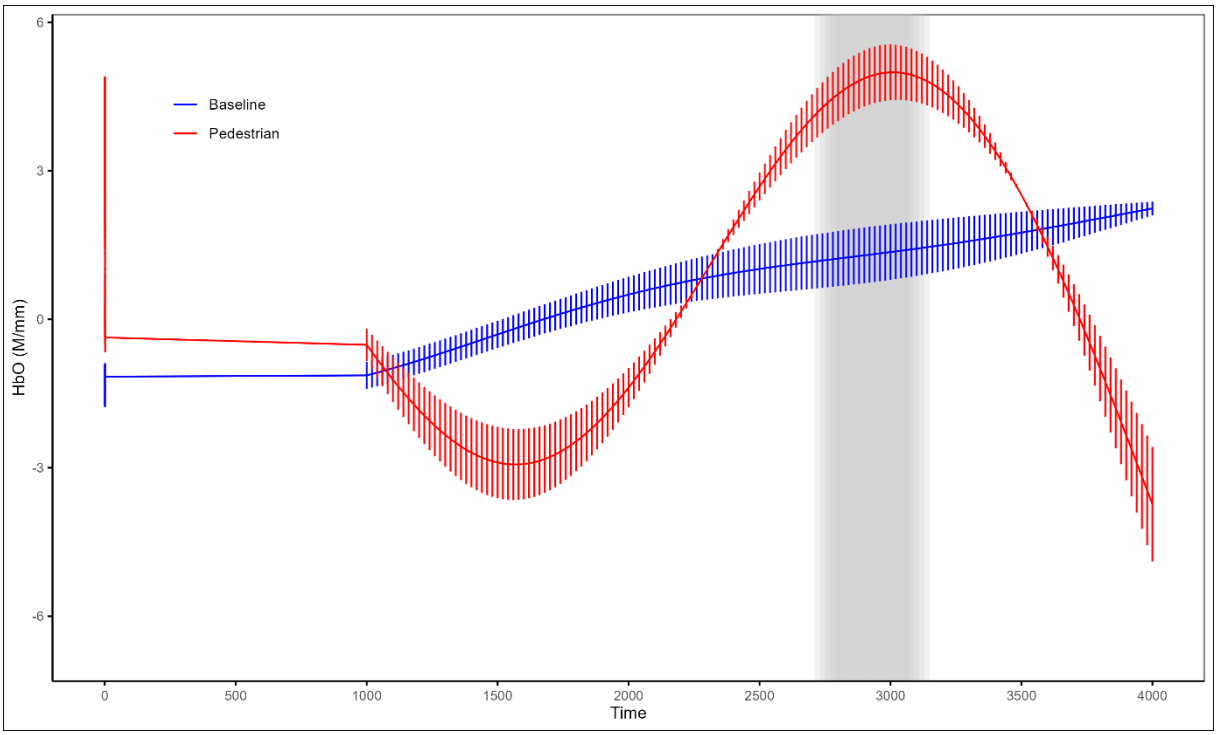

Note. The x-axis represents time in milliseconds (ms), with time point 0 indicating the onset of the event. Shaded areas represent time intervals where significant differences ($p < 0.05$) between Baseline and Pedestrian event were detected based on t-tests. Error bars indicate the standard error of the averaged signal.

For this time interval, the corresponding t-test results are detailed in Table 5. The table only shows the t-test results for the time points where there was a significant difference between the Pedestrian event and Baseline. During the interval where we found a significant difference, the HbO HRF values for the Pedestrian event were higher than those for Baseline. This means there was more activity, and therefore more cognitive load, in the right-DLPFC during the Pedestrian event compared to when no event was happening.

Table 5

Results from T-tests Comparing Event Pedestrian with Baseline for the Right-DLPFC

Time Point (ms)	Mean Pedestrian (M/mm)	Mean Baseline (M/mm)	t-value	p-value
2760	4,375	1,200	14,432	0,044
2780	4,467	1,213	20,288	0,031
2800	4,551	1,226	30,884	0,020
2820	4,629	1,239	54,635	0,011
2840	4,700	1,252	145,803	0,004
2860	4,763	1,265	472,097	0,001
2880	4,819	1,279	114,124	0,005
2900	4,867	1,292	75,922	0,008
2920	4,908	1,305	64,862	0,009
2940	4,940	1,318	64,346	0,009
2960	4,965	1,331	73,753	0,008
2980	4,981	1,345	105,609	0,006
3000	4,990	1,358	309,332	0,002
3020	4,989	1,372	192,031	0,003
3040	4,981	1,385	62,736	0,010
3060	4,964	1,399	34,377	0,018
3080	4,939	1,413	22,316	0,028
3100	4,905	1,427	15,797	0,040

Dynamic Route Features: Left-DLPFC

Significant differences ($p < 0.05$) in hemoglobin oxygenation levels were also found for the Pedestrian event with Baseline at the left-DLPFC, but for two time intervals. As shown in Figure 8, the significant difference in HbO HRF values appeared between time points 2600 and 2640, and between time points 3320 and 3360. These two intervals are marked with shaded areas in Figure 8.

Figure 8

Comparing Event Pedestrian with Baseline at the Left-DLPFC

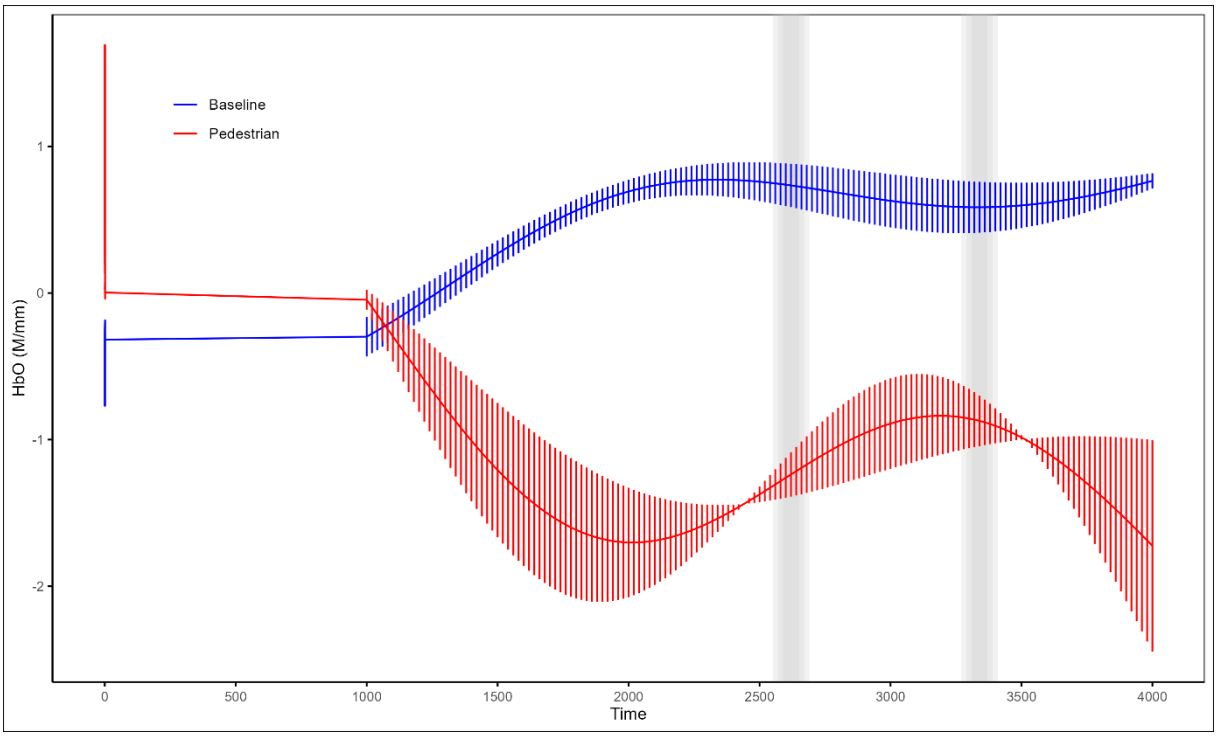

Note. The x-axis represents time in milliseconds (ms), with time point 0 indicating the onset of the event. Shaded areas represent time intervals where significant differences ($p < 0.05$) between Baseline and Pedestrian event were detected based on t-tests. Error bars indicate the standard error of the averaged signal.

The corresponding t-test results for these intervals are summarized in Table 6. The table only shows the t-test results for the time points where there was a significant difference between the Pedestrian event and Baseline. During both time intervals where we found a

significant difference, the HbO HRF values for the Pedestrian event were lower than those for Baseline. This means there was less activity, and therefore less cognitive load, in the left-DLPFC during the Pedestrian event compared to when no event was happening.

Table 6

Results from T-tests Comparing Event Pedestrian with Baseline for the Left-DLPFC

Time Point (ms)	Mean Pedestrian (M/mm)	Mean Baseline (M/mm)	t-value	p-value
2600	-1,260	0,738	-29,719	0,021
2620	-1,237	0,733	-88,349	0,007
2640	-1,215	0,728	-17,907	0,035
3320	-0,863	0,584	-16,198	0,039
3340	-0,872	0,584	-146,477	0,004
3360	-0,882	0,585	-12,794	0,049

For the Avoiding Object event at the left-DLPFC, a significant difference ($p < 0.05$) in HbO HRF means with Baseline in M/mm was found for time points 2820 to 3160, as indicated by the shaded area in Figure 9.

Figure 9

Comparing Event Avoiding Object with Baseline at the Left-DLPFC

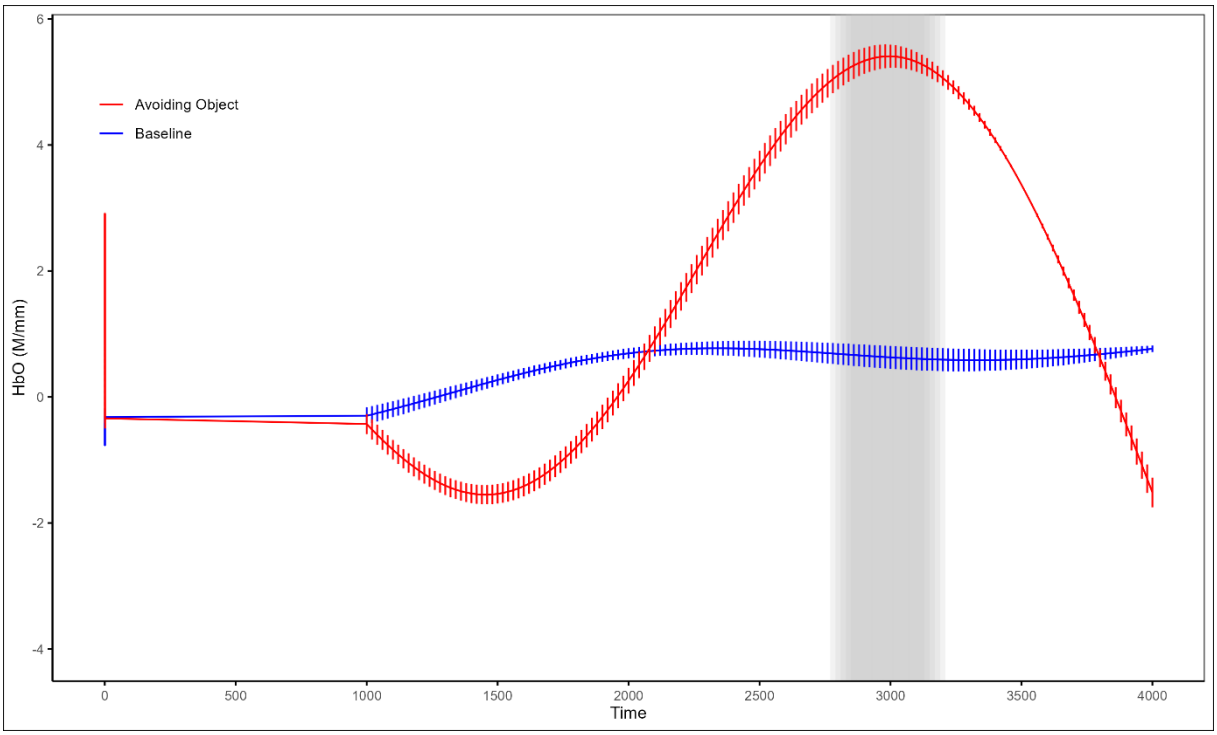

Note. The x-axis represents time in milliseconds (ms), with time point 0 indicating the onset of the event. Shaded areas represent time intervals where significant differences ($p < 0.05$) between Baseline and Avoiding Object event were detected based on t-tests. Error bars indicate the standard error of the averaged signal.

The corresponding t-test results are presented in Table 7. The table only shows the t-test results for the time points where there was a significant difference between the Avoiding Object event and Baseline. During the interval where we found a significant difference, the HbO HRF values for the Avoiding Object event were higher than those for Baseline. This means there was more activity, and therefore more cognitive load, in the left-DLPFC during the Avoiding Object event compared to when no event was happening.

Table 7

Results from T-tests Comparing Event Avoiding Object with Baseline for the Left-DLPFC

Time Point (ms)	Mean Avoiding Object (M/mm)	Mean Baseline (M/mm)	t-value	p-value
2820	5,166	0,678	12,739	0,049
2840	5,217	0,672	14,322	0,044
2860	5,263	0,666	16,321	0,038
2880	5,302	0,660	18,934	0,033
2900	5,336	0,655	22,508	0,028
2920	5,363	0,649	27,714	0,022
2940	5,384	0,644	36,032	0,017
2960	5,399	0,638	51,517	0,012
2980	5,407	0,633	90,666	0,007
3000	5,408	0,628	386,922	0,001
3020	5,404	0,624	167,934	0,003
3040	5,392	0,619	68,414	0,009
3060	5,374	0,615	42,680	0,014
3080	5,349	0,611	30,835	0,020
3100	5,318	0,607	24,009	0,026
3120	5,280	0,603	19,558	0,032
3140	5,236	0,600	16,419	0,038
3160	5,185	0,597	14,080	0,045

For the dynamic route features, no other significant differences in hemoglobin oxygenation levels between Baseline and any of the other events were found.

Connectivity Analysis Results

The connectivity analysis results, represented by correlation matrices between all channels for each event and Baseline, are provided in Appendix C. For each event and Baseline, two plots visualize the connectivity between channels. The left plot shows the connectivity between channels from a top-down (axial) view. Light grey lines signify correlations with a coefficient up to 0.3. Grey lines signify correlations with a coefficient of 0.3 to 0.8. Black lines signify correlations with a coefficient of 0.8 or higher. The colors of the nodes indicate different regions of the PFC: dorsolateral PFC (DLPFC), dorsomedial PFC (DMPFC), ventromedial PFC (VMPFC), and orbitofrontal cortex (OFC). The right plot shows the connectivity from an anterior view on a topographical map. Only correlations with a coefficient of 0.3 or higher are shown.

As illustrated in Figure 10, the connectivity of Baseline showed weak correlations of up to 0.3 and medium correlations from 0.3 to 0.8. No strong correlations were observed. Medium-strength correlations were clustered around the frontal area of the PFC but showed a broad network throughout the PFC. This suggested that multiple areas of the PFC were activated together when no event was happening during cycling. The strongest correlation coefficient in Baseline was $r = 0.578$.

Figure 10

Connectivity Plots of Baseline

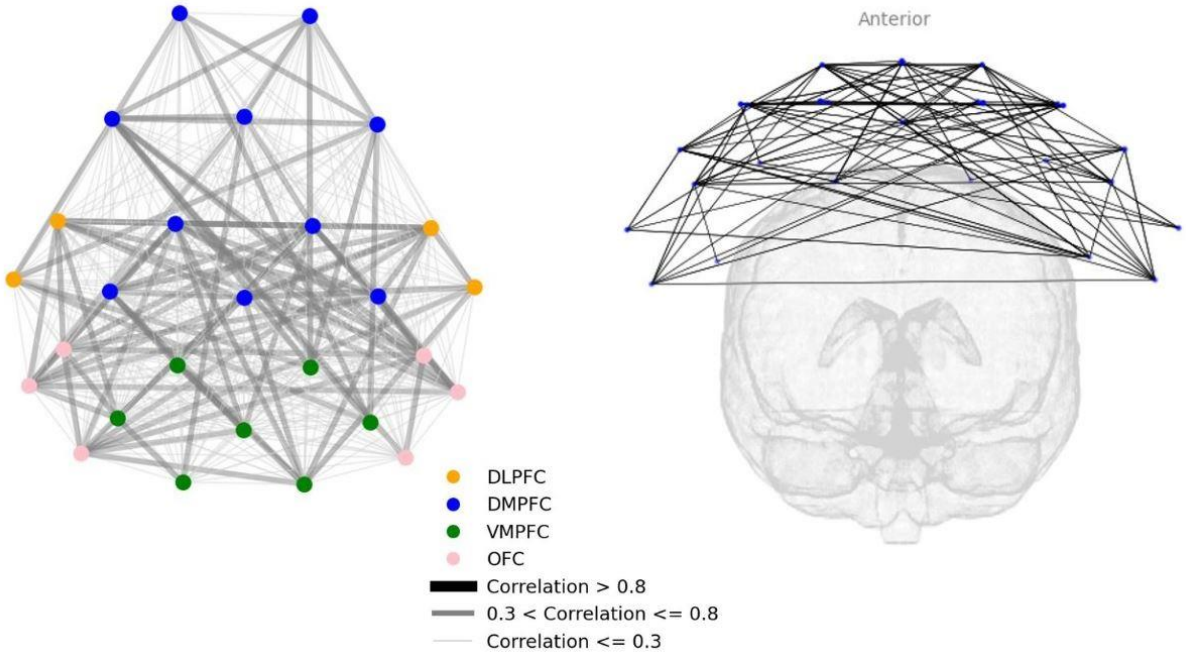

For the Avoiding Objects event, many weak correlations were observed, with few correlations of medium strength and no strong correlations, as depicted in Figure 11. Only the channels located at the left-DLPFC exhibited medium connectivity with a channel located at the right orbitofrontal cortex (OFC). Correlations of medium strength were focused on the dorsomedial prefrontal cortex (DMPFC). During this event, a more specific network seemed to be activated, with not all areas of the PFC being involved. The highest correlation coefficient for Avoiding Objects was r = 0.462.

Figure 11

Connectivity Plots of Avoiding Object Event

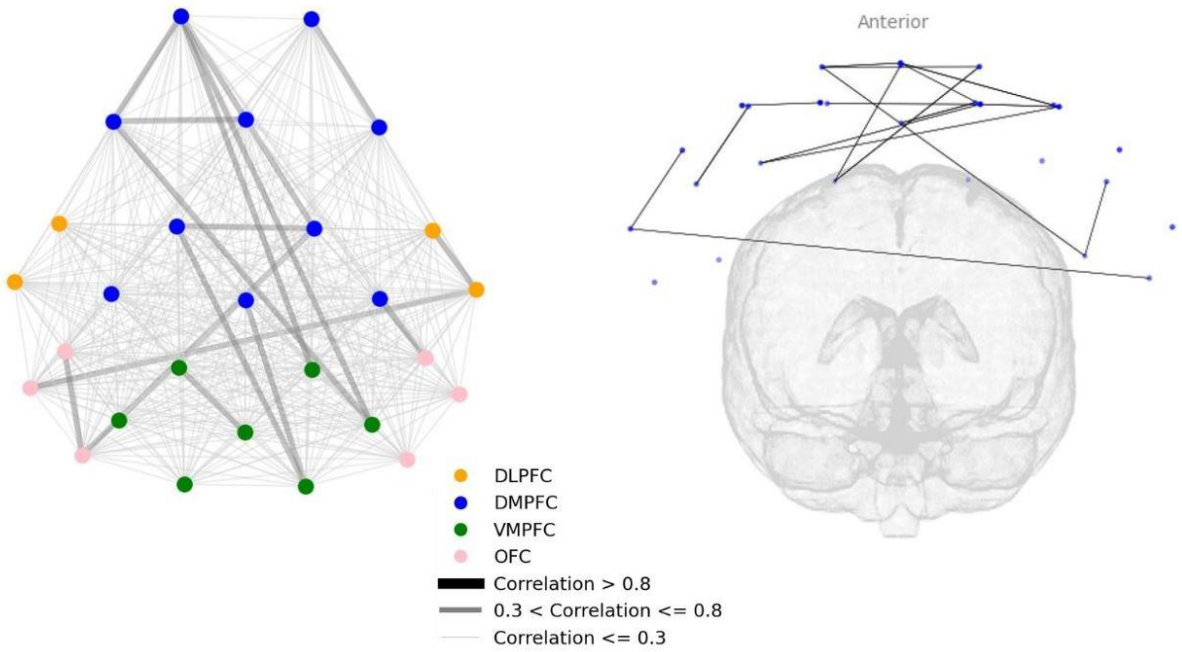

Similar patterns were observed for the Cyclist event, with predominantly weak or medium correlations and no strong correlations. The strongest correlation observed was r = 0.587. As shown in Figure 12, only the channels of the left-DLPFC had medium connectivity with channels from other areas, whereas the right-DLPFC had weak connections. The network for the Cycling event included all measured areas of the PFC, except for the right DLPFC, but had overall few connections of medium strength. This pointed towards a broad but less interactive network during this event.

Figure 12

Connectivity Plots of Cyclist Event

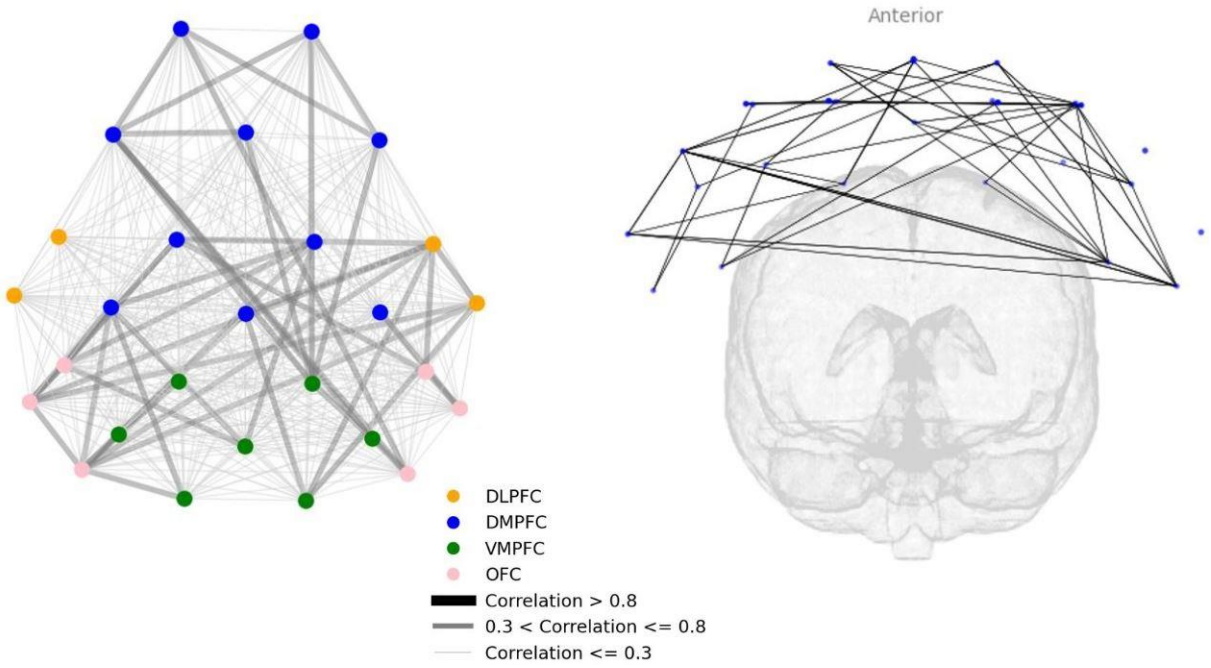

For the Crosswalk event condition, no strong correlations with a coefficient of 0.8 or higher were found. Mostly weak correlations up to 0.3 and fewer correlations with medium strength from 0.3 to 0.8 were observed. This can be seen in the right plot in Figure 13, which displays only medium or strong correlations. Most measured regions of the PFC were activated together, but there were few connections between the areas, indicating a less interactive network. The strongest correlation found for the Crosswalk event was r = 0.582.

Figure 13

Connectivity Plots of Crosswalk Event

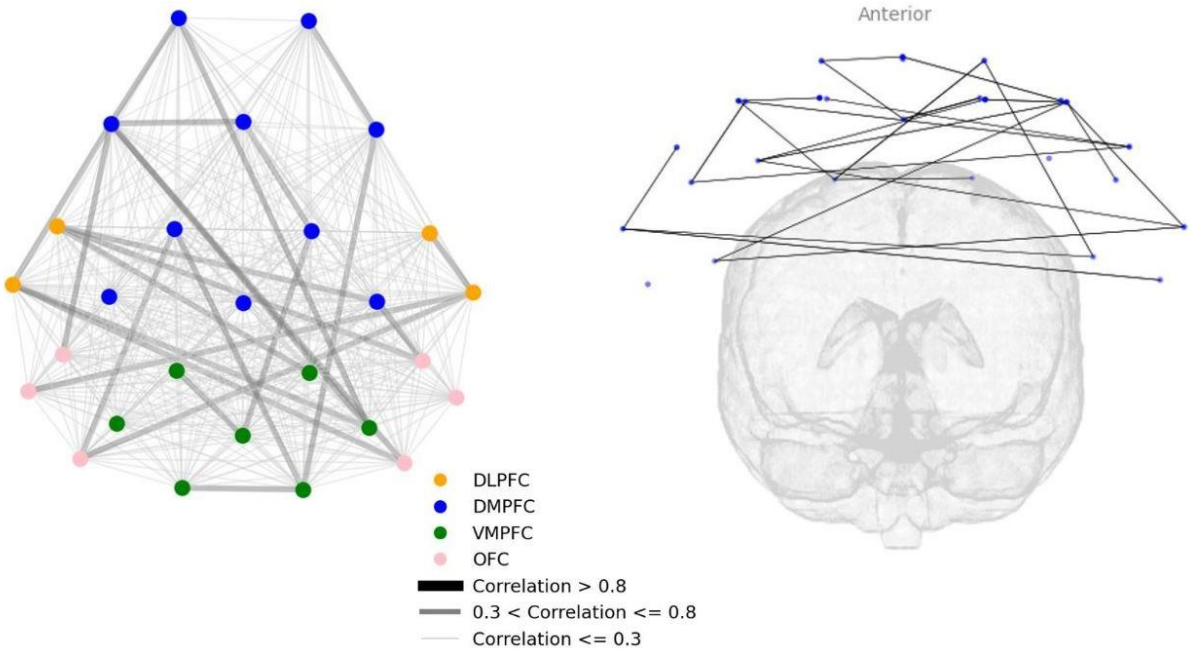

For the Intersection event, both weak and medium strength correlations were observed. All channels except for the two channels located at the right-DLPFC exhibited medium correlations with another channel, as shown in Figure 14. We observed a broad and relatively dense network for this event, with most measured PFC regions being activated together and interacting frequently. No strong correlation with a coefficient of 0.8 or higher was found, with the highest correlation coefficient for the Intersection event being r = 0.627.

Figure 14

Connectivity Plots for Intersection Event

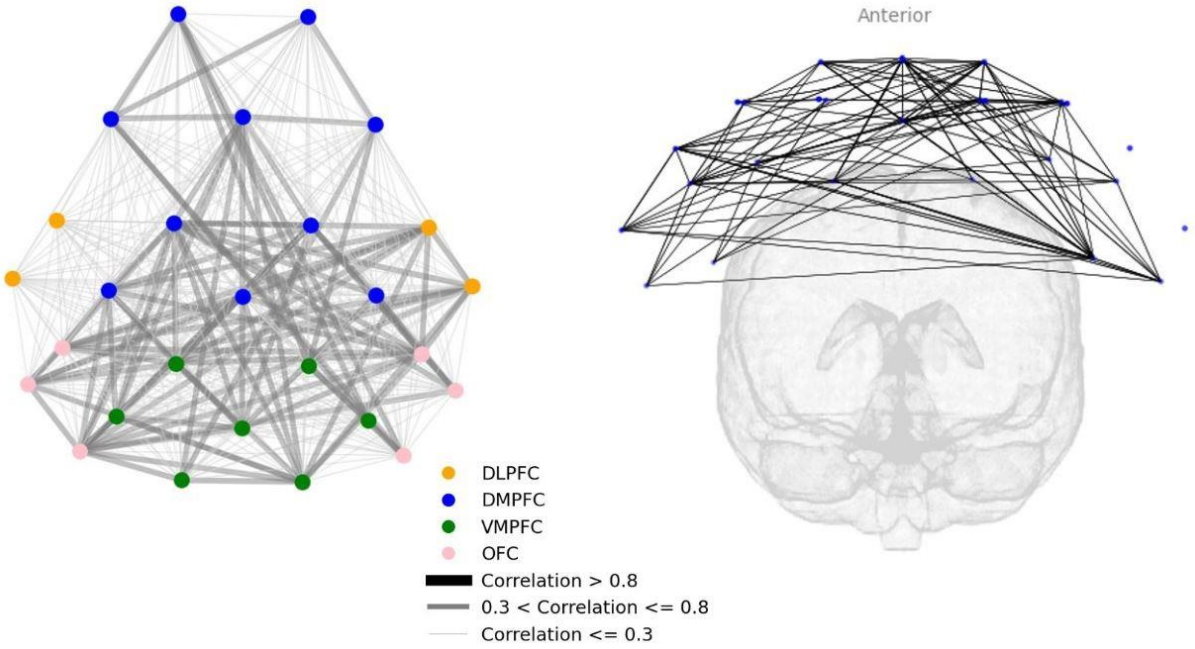

Similar to other events, weak and medium connections were observed for the Motorized Vehicle event, with no strong correlations. The plots in Figure 15 illustrate that connections of medium strength appeared to be focused on the left side of the PFC. The nodes located at the left-DLPFC had more medium correlations with other nodes than the nodes located at the right-DLPFC. This indicated that more regions in the left hemisphere were activated together during this event. The strongest correlation coefficient found for this event was r = 0.653.

Figure 15

Connectivity Plots for Motorized Vehicle Event

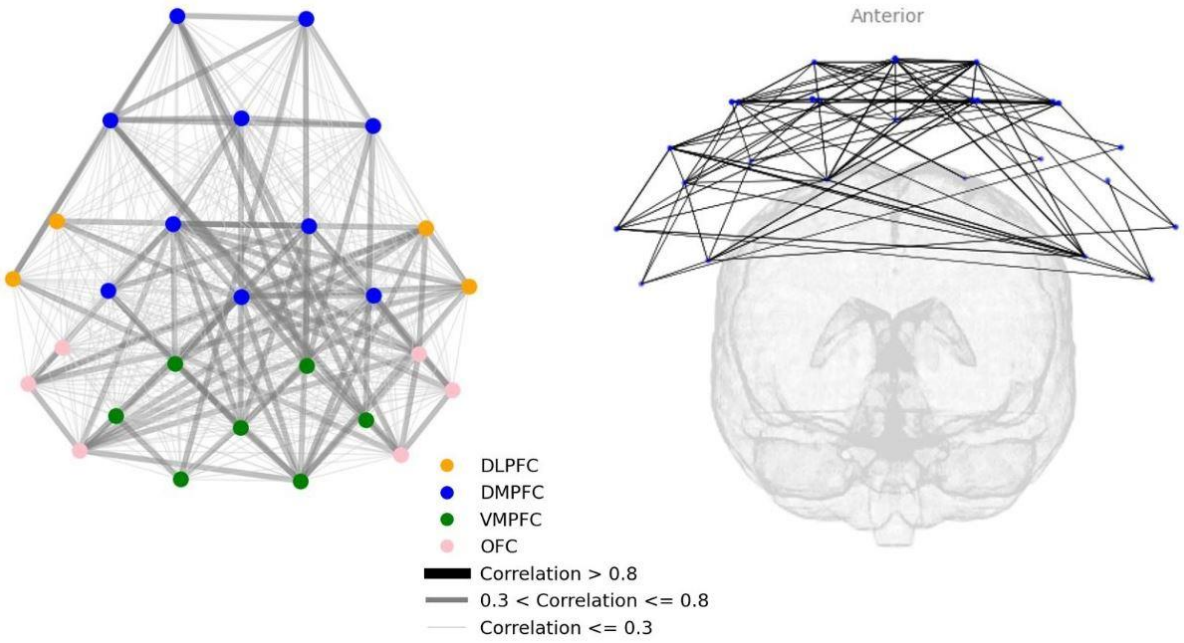

In the Pedestrian event condition, numerous weak and medium correlations were observed, but no strong correlations. This is evident in the plots of Figure 16, as the right plot shows many connectivity lines. The left plot illustrates that the medium connections were clustered in the frontal area of the PFC, in the frontal regions of the DMPFC and the ventromedial prefrontal cortex (VMPFC). The left-DLPFC had more medium correlations than the right-DLPFC. During the Pedestrian event, these above mentioned regions were activated simultaneously, and due to the dense network, they also showed frequent interactions. The strongest correlation coefficient of the Pedestrian event was r = 0.635.

Figure 16

Connectivity Plots for Pedestrian Event

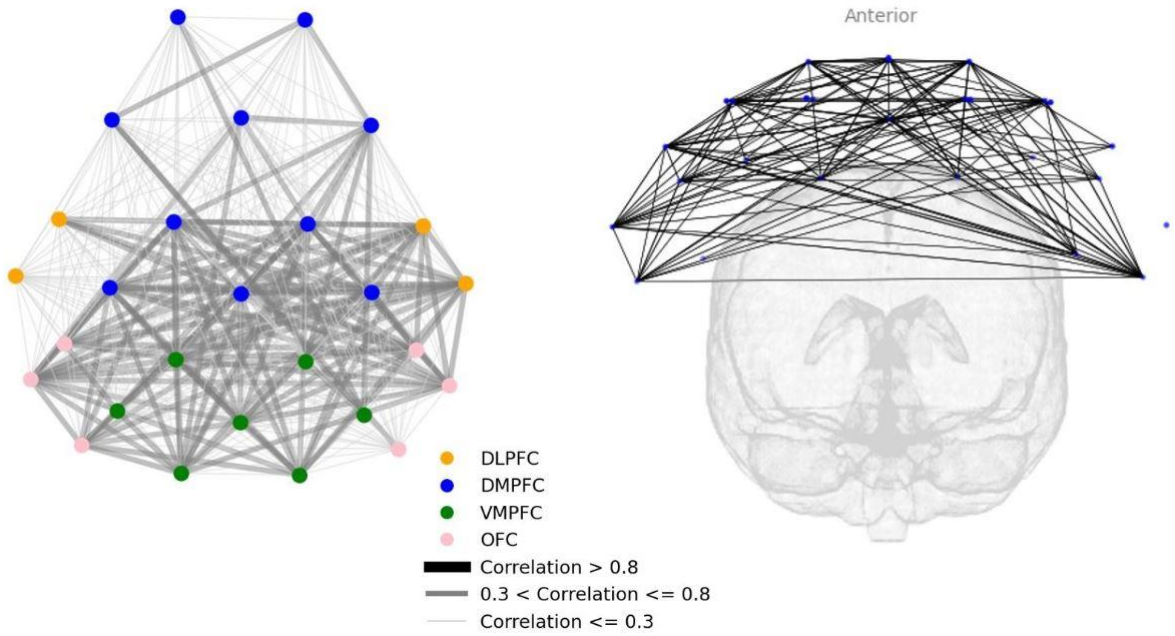

The Roundabout event mostly exhibited weak correlations of up to 0.3, few medium correlations from 0.3 to 0.8, and no strong correlations of 0.8 or higher, as depicted in Figure 17. The strongest connections for this event were located in the frontal regions of the PFC. For this event, we observed a specialized network where few regions of the PFC were activated, with minimal interactions between them. The strongest correlation coefficient for the Roundabout event was r = 0.426.

Figure 17

Connectivity Plots for Roundabout Event

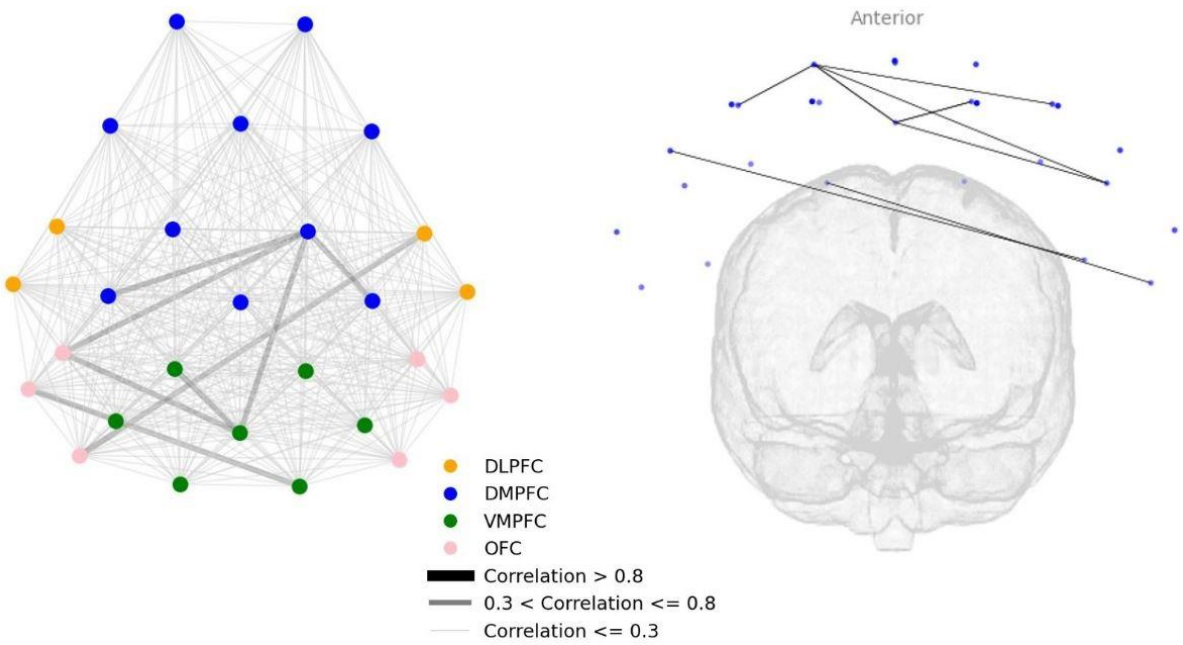

Similar to other events, the Traffic Light event exhibited weak and medium-strength connections with no strong connections, as depicted in Figure 18. The medium correlations appeared to be focused on the frontal area of the PFC, with no medium connections observed for the nodes located over the right-DLPFC. For the Traffic Light event, the network was overall broad, with most measured areas of the PFC being activated together, but the network was less dense, indicating less frequent interaction between the different regions. The strongest correlation coefficient found for the Traffic Light event was r = 0.502.

Figure 18

Connectivity Maps for Traffic Light Event

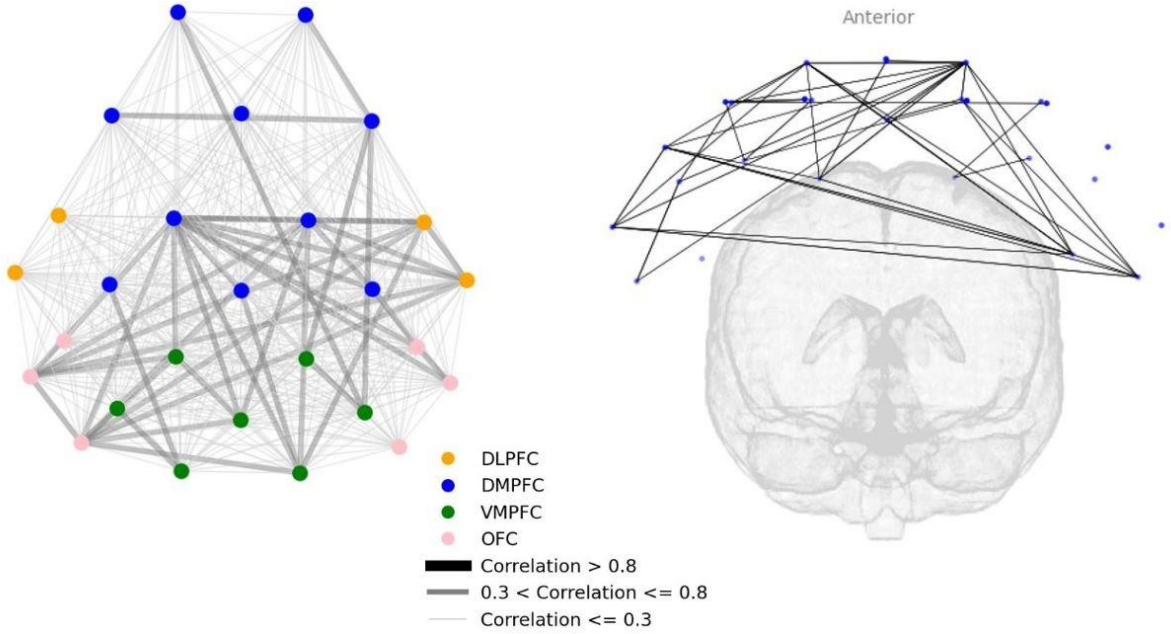

Discussion

The present study aimed to understand the patterns of cognitive load in cyclists across various events by examining when and how changes in activity patterns occur during cycling, identifying which route features coincide with changes in cognitive load, and exploring how connectivity within the PFC is affected by different traffic conditions.

Summary of Results

The results of the statistical analysis indicate that three of the eight events elicited increased cognitive load in participants. At the right-DLPFC, we find higher HbO levels for the crossing a crosswalk and viewing a pedestrian compared to Baseline, while at the left-DLPFC, HbO levels are higher for avoiding an object but lower for viewing a pedestrian compared to Baseline. Since viewing a pedestrian and avoiding an object are dynamic route features and crossing over a crosswalk is a static route feature, mostly dynamic route features coincide with a significant change in cognitive load. For all events that have a significant difference from Baseline, the interval where the difference was found occurs from almost three seconds to almost four seconds after the event onset, indicating that the increase or decrease in cognitive load occurs three to four seconds after encountering an event. We

anticipated this timing of change in HbO levels, as it aligns with the expected dynamics of the BOLD signal as observed in previous fMRI and fNIRS studies (Yeşilyurt et al., 2008; Hillman, 2014).

The results of the connectivity analysis indicate that for all events as well as Baseline, weak and medium connections are found, but no strong connections between the different areas of the PFC. The medium connections between the DLPFC, DMPFC, VMPFC, and OFC are quite evenly distributed for Baseline; however, a trend towards the frontal area of the DMPFC and the VMPFC can be observed (Figure 10). The same trend is observed across all of the eight events. Channels located in the frontal area of the DMPFC and the VMPFC have at least a few medium connections with other channels, even if there are few medium connections for a certain event. Another observation for all events except the Crosswalk event is that the right-DLPFC channels have no or fewer medium connections to other channels compared to the left-DLPFC channels. This cannot be observed for Baseline, where both sides of the DLPFC have medium connections with other channels. No difference in connectivity patterns between dynamic and static route features is detected, as all events exhibit similar trends.

When examining the networks of the strongest connections for each event and Baseline, Baseline shows a broad network involving all PFC regions (Figure 10). Passing through a roundabout has the smallest and least dense network, focused on the frontal DMPFC and VMPFC (Figure 17). Avoiding an object also targets these areas but with slightly more connections (Figure 11). Crossing a crosswalk engages more PFC areas than the previous events but has a less dense network than passing a cyclist or a traffic light (Figure 13). Passing a cyclist has a broader network than passing a traffic light, which is denser and focuses on the frontal DMPFC, VMPFC, and left-DLPFC (Figures 12, 18). Passing a motorized vehicle involves more PFC areas than the previous events but is less dense than going through an intersection and viewing a pedestrian (Figure 15). Going through an

intersection shows a broad and dense network, especially in the frontal DMPFC, VMPFC, and left-DLPFC (Figure 14). Viewing a pedestrian results in a less broad network than Baseline but has the densest network for the frontal DMPFC, VMPFC, and left-DLPFC among all events (Figure 16).

Interpretation of Statistical Analysis Results

As expected, and found in literature, we observe increased cognitive load for both static and dynamic route features, with a greater increase for dynamic route features (Foy and Chapman, 2018). Dynamic route features that elevate cognitive load in driving studies are associated with pedestrians, parked cars, and encountering cars or other cyclists (Foy and Chapman, 2018). Especially encountering pedestrians seems to be a factor coinciding with elevated load for car drivers, and in our study, we observe that it also elevates cognitive load for cyclists (Broadbent et al., 2023). Parked cars can be categorized similarly to the Avoiding Objects event, as both involve moving around an object obstructing one's path. We observe a significant increase in cognitive load, indicated by elevated HbO levels, for the Avoiding Object event. However, for the other dynamic route features (Motorized Vehicle and Cyclist), we do not observe a significant increase in cognitive load, despite previous research suggesting these features elevate cognitive load (Foy and Chapman, 2018).

When it comes to the static route features, we only find a significant increase in cognitive load when participants passed over a crosswalk (Figure 6), and not for other features such as traffic lights, intersections, and roundabouts. This is contradictory to previous research findings, as those features are part of urban road design, which is also thought to elicit an increase in cognitive load (Broadbent et al., 2023).

A unique activity pattern we find occurs for the Pedestrian event measured at the left-DLPFC. Here, instead of finding higher HbO levels for the Pedestrian event compared to Baseline, indicating increased cognitive load, we observe lower HbO levels for the Pedestrian event, meaning that cognitive load decreases. This is a unique activation pattern and an

unusual amplitude order compared to the significant increase in cognitive load found for the Pedestrian event at the right-DLPFC.

The study by Foy and Chapman (2018) found that prefrontal HbO levels increased when participants were driving on routes that included pedestrians. However, the effect of pedestrians on drivers is not well researched yet, since most driving studies do not include pedestrians (Oba et al., 2022). In driving studies involving pedestrians, researchers discovered that pedestrians act as external distractors, drawing the driver's attention. This is because viewing another person constitutes social information, triggering task-irrelevant processing that can impact cognitive load during driving (Oba et al., 2022). In another driving study, the highest increase in mental activity was observed in an anterior part of the PFC when participants faced the risk scenario of a pedestrian crossing the road, compared to other risk scenarios (Wang et al., 2023). Given that seeing a pedestrian leads to increased activity, it should correspond to a rise in cognitive load, as we observe in the right-DLPFC, rather than a decrease, as we see in the left-DLPFC. Another approach to explain this unique pattern is to look into the different roles of the two sides of the DLPFC. The left-DLPFC is primarily engaged in tasks demanding top-down cognitive control, such as planning and problem-solving (Allaert et al., 2019; Y. Wang et al., 2020). In contrast, the right-DLPFC is more associated with regulating emotions and attending to external stimuli, particularly during stress-inducing or vigilance-demanding tasks (Allaert et al., 2019; Y. Wang et al., 2020; Causse et al., 2017). This might explain why there is a significant increase in activity in the right-DLPFC, given that Oba et al. (2022) suggested pedestrians serve as distractors by capturing the driver’s attention. However, it is not specified whether the engagement of the right-DLPFC in attentional processes linked to external stimuli exerts an inhibitory effect on the left-DLPFC, leading to a decrease in its activity. Current research does not explain the observed effect on the left-DLPFC when observing a pedestrian; thus, further research is needed to understand this activity pattern.

Possible reasons for not observing an increase in cognitive load for the other five route features in this study could be attributed to the age range of participants, 19 to 35, with a mean age of 23 (Foy et al., 2016). Research suggests that reduced PFC activity is associated with PFC maturation, which is not complete until around 25 years of age. Older individuals typically exhibit greater changes in PFC activity compared to younger ones (Foy et al., 2016). Given our participants' mean age of 23, it is possible that many participants have not yet fully developed their PFC, resulting in reduced activity related to cognitive load. However, further evidence is needed to solidify this association (Foy et al., 2016).

Another explanation could be familiarity or automation. The participants, consisting of 17 students and faculty members from the University of Twente and Saxion Hogeschool in Enschede, the Netherlands (Chinpongsuwan, 2023), likely have a degree of familiarity with cycling in Enschede and its route infrastructure. Familiarity or experience with a task is known to reduce cognitive load (Wu et al., 2024), as experienced individuals can perform tasks more effortlessly (Stapel et al., 2019). Automated routines can make certain tasks less demanding, rendering them insensitive to changes in cognitive load (Stapel et al., 2019). Cycling the route multiple times may have made it a routine task for participants, thereby not resulting in an increased cognitive load.

Interpretation of Connectivity Analysis Results

In regard to the connectivity analysis, we are able to observe connectivity within the PFC. However, we do not find strong connections, which we anticipated since the PFC is heavily involved in cognitive load, and certain areas, such as the DLPFC, are known to play a significant role in connectivity during load (Fishburn et al., 2014; Zuo et al., 2019; Aydöre et al., 2010). We also find varying levels of connectivity for different events. Crossing an intersection and observing a pedestrian results in more medium connections compared to Baseline. However, avoiding objects, passing by a cyclist or motorized vehicle, crossing over

a crosswalk, navigating through a roundabout, or encountering a traffic light leads to fewer medium connections compared to Baseline.

However, we cannot definitively say that cognitive load is experienced in these situations, since in the statistical analysis, only a significant increase is found when avoiding an object, crossing over a crosswalk and viewing a pedestrian. We can, therefore, assume that while cycling, participants experience less connectivity in the brain when dealing with route features such as crosswalks and objects in their path, but more connectivity within the PFC when encountering pedestrians.

We can explain the increased connectivity and broader network by assuming that viewing a pedestrian while cycling activates more areas of the PFC simultaneously, likely due to the additional processing of social information, as discussed earlier (Oba et al., 2022).

The fewer medium connections and more specialised networks observed while avoiding an object in one's path and going over a crosswalk could be attributed to the possibility that fewer regions within the PFC are active simultaneously during those events. The lack of strong connections between any regions of the PFC could also be due to the fact that during cognitive load, even if there is connectivity within the PFC, there might be stronger connectivity between the PFC and other brain regions, especially those involved in executive functions (Zanto & Gazzaley, 2013). Brain regions often noted for having increased connectivity with the PFC during cognitive load include the parietal cortex, the premotor cortex, and the supplementary motor area (Nagel et al., 2011; Honey et al., 2002; Zanto & Gazzaley, 2013).

Another explanation for the lack of strong connections between different PFC regions could be insufficient activation due to incomplete PFC maturation, as discussed earlier (Foy et al., 2016).

An interesting observation made during the connectivity analysis is that the right-DLPFC has fewer or no medium connections to other areas of the PFC during the different

events compared to the left-DLPFC. We know that the left and right-DLPFC have slightly different roles when it comes to cognitive load, but both are involved in cognitive load (Lim et al., 2020). Under cognitive load, different networks in the brain become active, one of them being the frontoparietal executive control network (FPN), which the DLPFC belongs to (Zuo et al., 2019). We can assume that perhaps the left-DLPFC is more connected to other areas of the PFC during cognitive load, whereas the right-DLPFC is more connected to areas outside of the PFC. There is no research available about the differentiation in connectivity between the right and left-DLPFC during cognitive workload, so this remains speculative.

Practical Implications

The practical implications of this study suggest that it is possible to assess cognitive load while cycling with an fNIRS device located at the PFC. Based on our findings, we can assume that dynamic route features may impact cyclists' level of cognitive load more than road infrastructure. Especially when engaging with pedestrians, it appears that this interaction has a significant impact on cyclists' cognitive load, similar to encountering an object in their path or passing over a crosswalk. It seems that the chance of someone or something entering the path they are cycling on, whether it is an object or a person, increases their cognitive load. This knowledge can inform safety measures for infrastructure design. For instance, since sidewalks are often next to cycling paths, a barrier such as a grass strip could be placed between them to keep pedestrians and cyclists apart, thereby reducing the chance of a pedestrian stepping onto the cycling path. Additionally, ensuring that cycling paths are always separate from roads used by cars and other motorized vehicles, and prohibiting parking on the side of the road where cycling paths are located, could help reduce the cognitive load on cyclists.

Limitations and Future Directions

It is important to acknowledge that besides the practical implications, this study also has a few limitations. Data was collected from optodes located at the PFC; however, it is

possible that the optodes did not cover the whole PFC. Areas such as the ventrolateral PFC, which might also be involved in cognitive workload, were not included in the analysis as they lie outside of the optode placement (Nagel et al., 2011). Furthermore, the different areas of the PFC and their corresponding optode placements were only estimated since there is no guideline on which optode placement corresponds to which exact brain area for the fNIRS device and the optode template used for data collection. Another important limitation of this study is that not all participants encountered the Crosswalk and Avoiding Object events. Therefore, the sample sizes for these two events are smaller than for the other events, which could potentially reduce the reliability of the results for these two events. This is important to acknowledge since we did find significant changes in cognitive load for these two events. Ensuring that all participants encounter the same events can only be done in simulators, but that would compromise the authenticity. While t-tests and correlation analyses offered some valuable insights into how cognitive load relates to encountering various route features while cycling in this study, they can oversimplify the dynamics of brain activity and functional connectivity. These methods may not fully capture the complexity of neural interactions and could miss nuanced patterns that might be better explored using advanced multivariate techniques or network analyses.

Future studies should replicate the study to determine whether the unusual activity pattern for the Pedestrian event at the left-DLPFC is a recurring pattern or just an anomaly found in our study. Since the effect of pedestrians on drivers or cyclists is not well-researched, more research on this would be beneficial. Another interesting aspect to explore would be to conduct the same study with young adults and older adults to see whether older adults experience more changes in cognitive load for the different route features compared to young adults, and whether PFC maturation is a plausible explanation for not finding many significant changes in cognitive load in our study. It would also be beneficial to select an fNIRS device or optode template where the exact brain regions corresponding to each optode

position are known, making it easier to draw conclusions about connections between specific brain regions in a connectivity analysis. Another interesting area to explore is the application of a brain-computer interface or neurofeedback for managing cognitive load in cyclists. By providing real-time feedback on brain activity, these technologies could help cyclists monitor and adjust their cognitive load in response to different route features, potentially improving safety.

Conclusion

This study aimed to understand cognitive load patterns in cyclists by examining changes in activity during various cycling events, identifying route features that coincide with these changes, and exploring connectivity within the PFC under different traffic conditions. Our findings revealed that dynamic route features, such as avoiding an object and viewing a pedestrian, generally led to an increase in cognitive load, as evidenced by higher HbO levels in the right-DLPFC and left-DLPFC. Static route features like crossing a crosswalk also elicited increased cognitive load, but to a lesser extent than dynamic features. The connectivity analysis showed weak to medium connections within the PFC across all events, with notable connectivity in the frontal areas of the DMPFC and VMPFC. Interestingly, the right-DLPFC exhibited fewer medium connections compared to the left-DLPFC during events, which might suggest a differentiation in functional roles under cognitive load. Our results align with previous research indicating that dynamic route features, particularly those involving potential social interactions like viewing pedestrians, significantly impact cognitive load. However, the unique decrease in cognitive load observed in the left-DLPFC when viewing pedestrians requires further investigation to understand the underlying neural mechanisms. This study underscores the importance of considering cognitive load in urban planning and infrastructure design to enhance cyclist safety. Measures such as separating cycling paths from sidewalks and roads could potentially reduce cognitive load and improve the overall cycling safety. Future research should address the limitations identified, including

exploring the role of PFC maturation and employing advanced neuroimaging techniques to capture the complexity of neural interactions. Additionally, investigating the use of brain-computer interfaces or neurofeedback for real-time management of cognitive load in cyclists presents an exciting avenue for improving cycling safety and performance.

References

Adam, L., Jones, T., & Brömmelstroet, M. T. (2018). Planning for cycling in the dispersed city: establishing a hierarchy of effectiveness of municipal cycling policies. *Transportation*, *47*(2), 503–527. https://doi.org/10.1007/s11116-018-9878-3

Allaert, J., Sanchez-Lopez, A., De Raedt, R., Baeken, C., & Vanderhasselt, M. (2019). Inverse effects of tDCS over the left versus right DLPC on emotional processing: A pupillometry study. *PloS One*, *14*(6), e0218327. https://doi.org/10.1371/journal.pone.0218327

Arsalidou, M., Pascual-Leone, J., Johnson, J., Morris, D., & Taylor, M. J. (2013). A balancing act of the brain: activations and deactivations driven by cognitive load. *Brain and Behavior*, *3*(3), 273–285. https://doi.org/10.1002/brb3.128

Artinis Medical Systems. (2024, May 17). *How to: Start a measurement and do a short analysis — Artinis Medical Systems | (f)NIRS devices*. Artinis Medical Systems | (F)NIRS Devices. Retrieved June 17, 2024, from https://www.artinis.com/blogpost-all/2020/how-to-start-a-measurement-and-do-a-short-analysis

Aydöre, S., Mihak, M., Cifti, K., & Akin, A. (2010). On temporal connectivity of PFC via Gauss - Markov modeling of FNIRS signals. *IEEE Transactions on Bio-medical Engineering/IEEE Transactions on Biomedical Engineering*, *57*(3), 761–768. https://doi.org/10.1109/tbme.2009.2020792

Bastos, A. M., & Schoffelen, J. (2016). A tutorial review of functional connectivity analysis methods and their interpretational pitfalls. *Frontiers in Systems Neuroscience*, *9*. https://doi.org/10.3389/fnsys.2015.00175

Bishop, A., MacNeil, E., & İzzetoğlu, K. (2021). Cognitive workload quantified by physiological sensors in realistic immersive settings. In *Lecture notes in computer science* (pp. 119–133). https://doi.org/10.1007/978-3-030-78114-9_9

Broadbent, D. P., D'Innocenzo, G., Ellmers, T. J., Parsler, J., Szameitat, A. J., & Bishop, D. (2023). Cognitive load, working memory capacity and driving performance: A preliminary fNIRS and eye tracking study. *Transportation Research Part F-traffic Psychology and Behaviour*, *92*, 121–132. https://doi.org/10.1016/j.trf.2022.11.013

Bunce, S. C., İzzetoğlu, K., Ayaz, H., Shewokis, P. A., İzzetoğlu, M., Pourrezaei, K., & Onaral, B. (2011). Implementation of FNIRS for monitoring levels of expertise and mental workload. In *Lecture notes in computer science* (pp. 13–22). https://doi.org/10.1007/978-3-642-21852-1_2

Causse, M., Chua, Z. K., Peysakhovich, V., Del Campo, N., & Matton, N. (2017). Mental workload and neural efficiency quantified in the prefrontal cortex using fNIRS. *Scientific Reports*, *7*(1). https://doi.org/10.1038/s41598-017-05378-x

Chinpongsuwan, P. (2023). *Unravelling the mind of cyclists: Exploring the potential of fNIRS in capturing subjective cycling experiences* [BSc thesis]. University of Twente.

Cycling safety. (2012b). In *The MIT Press eBooks*. https://doi.org/10.7551/mitpress/9434.003.0010

Dans, P. W., Foglia, S. D., & Nelson, A. J. (2021). Data processing in Functional Near-Infrared Spectroscopy (FNIRS) motor control research. *Brain Sciences*, *11*(5), 606. https://doi.org/10.3390/brainsci11050606

Dimitrakopoulos, G. N., Kakkos, I., Anastasiou, A., Bezerianos, A., Sun, Y., & Matsopoulos, G. K. (2023). Cognitive reorganization due to mental workload: A functional connectivity analysis based on working memory paradigms. *Applied Sciences*, *13*(4), 2129. https://doi.org/10.3390/app13042129

Dominguez, M., MD. (2019, May 20). *Cerebral Cortex - Neurology - Medbullets Step 1*. Medbullets Step 1. Retrieved June 17, 2024, from https://step1.medbullets.com/neurology/113013/cerebral-cortex

Engström, J., Johansson, E., & Östlund, J. (2005). Effects of visual and cognitive load in real and simulated motorway driving. *Transportation Research Part F: Traffic Psychology and Behaviour*, *8*(2), 97–120. https://doi.org/10.1016/j.trf.2005.04.012

Engström, J., Markkula, G., Victor, T., & Merat, N. (2017). Effects of cognitive load on driving performance: The Cognitive Control Hypothesis. *Human Factors*, *59*(5), 734–764. https://doi.org/10.1177/0018720817690639

Fanton, S., & Thompson, W. H. (2023). NetPlotBrain: A Python package for visualizing networks and brains. *Network Neuroscience*, *7*(2), 461–477. https://doi.org/10.1162/netn_a_00313

Fishburn, F. A., Norr, M. E., Medvedev, A. V., & Vaidya, C. J. (2014). Sensitivity of fNIRS to cognitive state and load. *Frontiers in Human Neuroscience*, *8*. https://doi.org/10.3389/fnhum.2014.00076

Foy, H. J., & Chapman, P. (2018). Mental workload is reflected in driver behaviour, physiology, eye movements and prefrontal cortex activation. *Applied Ergonomics*, *73*, 90–99. https://doi.org/10.1016/j.apergo.2018.06.006

Foy, H. J., Runham, P., & Chapman, P. (2016). Prefrontal cortex activation and young driver behaviour: a FNIRS study. *PLOS ONE*, *11*(5), e0156512. https://doi.org/10.1371/journal.pone.0156512

Fraser, S., & Lock, K. (2010). Cycling for transport and public health: a systematic review of the effect of the environment on cycling. *European Journal of Public Health*, *21*(6), 738–743. https://doi.org/10.1093/eurpub/ckq145

Hillman, E. M. (2014). Coupling mechanism and significance of the BOLD Signal: a status report. *Annual Review of Neuroscience*, *37*(1), 161–181. https://doi.org/10.1146/annurev-neuro-071013-014111

Honey, G., Fu, C., Kim, J., Brammer, M., Croudace, T., Suckling, J., Pich, E., Williams, S., & Bullmore, E. (2002). Effects of verbal working memory load on corticocortical

connectivity modeled by path analysis of functional magnetic resonance imaging data. *NeuroImage*, *17*(2), 573–582. https://doi.org/10.1006/nimg.2002.1193

Horton, D., Rosen, P. P., & Cox, P. (2016). Cycling and society. In *Routledge eBooks*. https://doi.org/10.4324/9781315575735

Hunter, J. D. (2007). MatPlotLib: a 2D Graphics environment. *Computing in Science & Engineering*, *9*(3), 90–95. https://doi.org/10.1109/mcse.2007.55

Huppert, T. J., Diamond, S. G., Franceschini, M. A., & Boas, D. A. (2009). HomER: a review of time-series analysis methods for near-infrared spectroscopy of the brain. Applied Optics, 48(10), D280. https://doi.org/10.1364/ao.48.00d280

Juhra, C., Wieskötter, B., Chu, K., Trost, L., Weiß, U., Messerschmidt, M., Malczyk, A., Heckwolf, M. J., & Raschke, M. J. (2012). Bicycle accidents – Do we only see the tip of the iceberg? *Injury-International Journal of the Care of the Injured*, *43*(12), 2026–2034. https://doi.org/10.1016/j.injury.2011.10.016

Lee, Y., Lee, J. D., & Boyle, L. N. (2009). The interaction of Cognitive load and Attention-Directing cues in driving. *Human Factors*, *51*(3), 271–280. https://doi.org/10.1177/0018720809337814

Lim, L. G., Ung, W. C., Chan, Y. L., Lu, C., Sutoko, S., Funane, T., Kiguchi, M., & Tang, T. B. (2020). A unified analytical framework with multiple FNIRS features for mental workload assessment in the prefrontal cortex. *IEEE Transactions on Neural Systems and Rehabilitation Engineering*, *28*(11), 2367–2376. https://doi.org/10.1109/tnsre.2020.3026991

Liu, Z., Zhang, M., Xu, G., Huo, C., Tan, Q., Li, Z., & Yuan, Q. (2017). Effective Connectivity Analysis of the Brain Network in Drivers during Actual Driving Using Near-Infrared Spectroscopy. *Frontiers in Behavioral Neuroscience*, *11*. https://doi.org/10.3389/fnbeh.2017.00211

Nagel, I. E., Preuschhof, C., Li, S., Nyberg, L., Bäckman, L., Lindenberger, U., & Heekeren, H. R. (2011). Load modulation of BOLD response and connectivity predicts working memory performance in younger and older adults. *Journal of Cognitive Neuroscience*, *23*(8), 2030–2045. https://doi.org/10.1162/jocn.2010.21560

Nilsson, E., Aust, M. L., Engström, J., Svanberg, B., & Lindén, P. (2018). Effects of cognitive load on response time in an unexpected lead vehicle braking scenario and the detection response task (DRT). *Transportation Research Part F-traffic Psychology and Behaviour*, *59*, 463–474. https://doi.org/10.1016/j.trf.2018.09.026

Oba, K., Hamada, K., Tanabe-Ishibashi, A., Murase, F., Hirose, M., Kawashima, R., & Sugiura, M. (2022). Neural Correlates Predicting Lane-Keeping and Hazard Detection: An FMRI study featuring a Pedestrian-Rich simulator environment. *Frontiers in Human Neuroscience, 16*. https://doi.org/10.3389/fnhum.2022.754379

Peck, E. M., Afergan, D., Yuksel, B. F., Lalooses, F., & Jacob, R. J. K. (2014). Using FNIRS to measure mental workload in the real world. In *Human-computer interaction series* (pp. 117–139). https://doi.org/10.1007/978-1-4471-6392-3_6

Pinti, P., Scholkmann, F., Hamilton, A., Burgess, P., & Tachtsidis, I. (2019). Current status and issues regarding pre-processing of FNIRS Neuroimaging Data: An investigation of diverse signal filtering methods within a general linear model framework. *Frontiers in Human Neuroscience, 12*. https://doi.org/10.3389/fnhum.2018.00505

Python Software Foundation. (2021). *Python* (Version 3.10.11) [Software]. Python Software Foundation. https://www.python.org/

Reyes, M. L., & Lee, J. D. (2008). Effects of cognitive load presence and duration on driver eye movements and event detection performance. *Transportation Research Part F: Traffic Psychology and Behaviour*, *11*(6), 391–402. https://doi.org/10.1016/j.trf.2008.03.004

RStudio Team (2024). *R: a language and environment for statistical computing*. R Foundation for Statistical Computing, Vienna, Austria. https://www.R-project.org

Stapel, J., Mullakkal-Babu, F. A., & Happee, R. (2019). Automated driving reduces perceived workload, but monitoring causes higher cognitive load than manual driving. *Transportation Research. Part F, Traffic Psychology and Behaviour*, *60*, 590–605. https://doi.org/10.1016/j.trf.2018.11.006

Unni, A., Ihme, K., Surm, H., Weber, L., Lüdtke, A., Nicklas, D., Jipp, M., & Rieger, J. W. (2015). Brain activity measured with fNIRS for the prediction of cognitive workload. *6th IEEE International Conference on Cognitive Infocommunications*. https://doi.org/10.1109/coginfocom.2015.7390617

Wang, H., Zhang, X., Li, J., Li, B., Gao, X., Hao, Z., Fu, J., Zhou, Z., & Atia, M. (2023). Driving risk cognition of passengers in highly automated driving based on the prefrontal cortex activity via fNIRS. *Scientific Reports*, *13*(1). https://doi.org/10.1038/s41598-023-41549-9

Wang, Y., Cao, N., Lin, Y., Chen, R., & Zhang, J. (2020). Hemispheric differences in functional interactions between the dorsal lateral prefrontal cortex and ipsilateral motor cortex. *Frontiers in Human Neuroscience*, *14*. https://doi.org/10.3389/fnhum.2020.00202

Wilcox, T., & Biondi, M. (2015). fNIRS in the developmental sciences. *Wiley Interdisciplinary Reviews. Cognitive Science*, *6*(3), 263–283. https://doi.org/10.1002/wcs.1343

Wu, Y., Zhang, Z., Zhang, Y., Zheng, B., & Aghazadeh, F. (2024). Pupil response in visual tracking tasks: the impacts of task load, familiarity, and gaze position. *Sensors*, *24*(8), 2545. https://doi.org/10.3390/s24082545

Yeşilyurt, B., Uğurbil, K., & Uludağ, K. (2008). Dynamics and nonlinearities of the BOLD response at very short stimulus durations. *Magnetic Resonance Imaging*, *26*(7), 853–862. https://doi.org/10.1016/j.mri.2008.01.008

Zanto, T. P., & Gazzaley, A. (2013). Fronto-parietal network: flexible hub of cognitive control. *Trends in Cognitive Sciences*, *17*(12), 602–603. https://doi.org/10.1016/j.tics.2013.10.001

Zuo, N., Salami, A., Yang, Y., Yang, Z., Sui, J., & Jiang, T. (2019). Activation-based association profiles differentiate network roles across cognitive loads. *Human Brain Mapping*, *40*(9), 2800–2812. https://doi.org/10.1002/hbm.24561

Appendix A

Statistical Analysis Plots of Unsignificant Results

Figure A1

Comparing Event Avoiding Object with Baseline at the Right-DLPFC

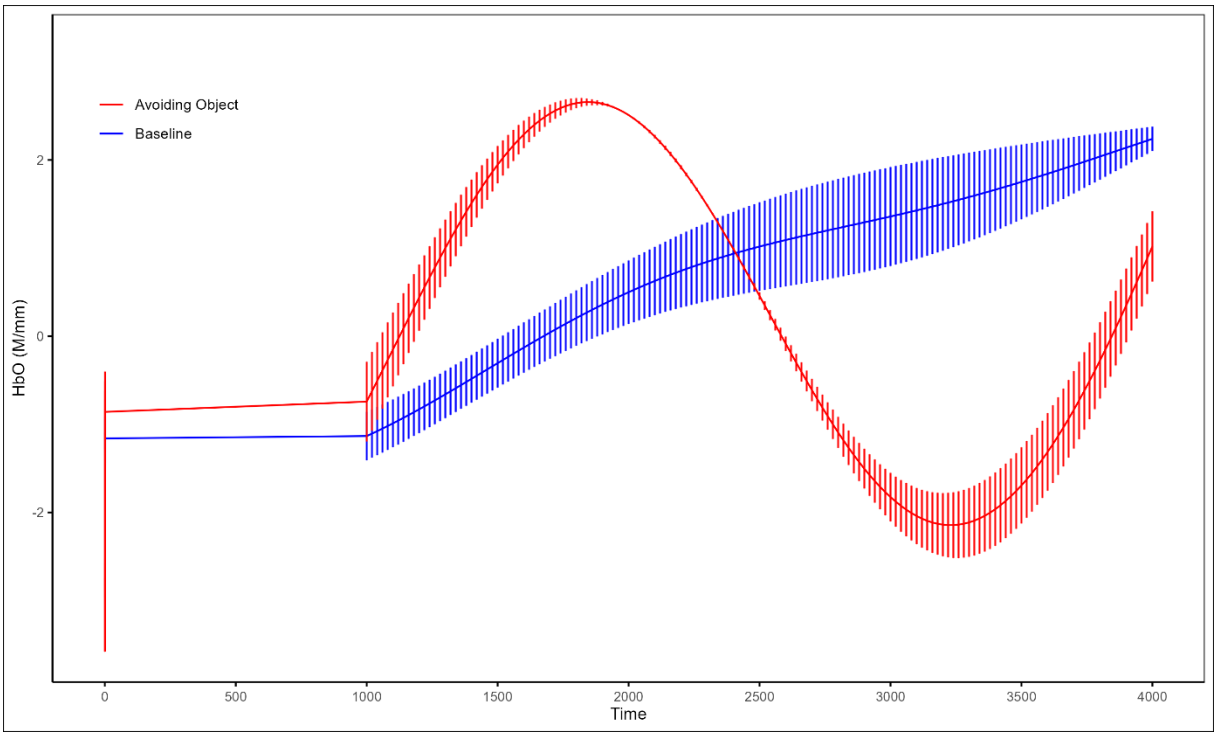

Figure A2

Comparing Event Cyclist with Baseline at the Right-DLPFC

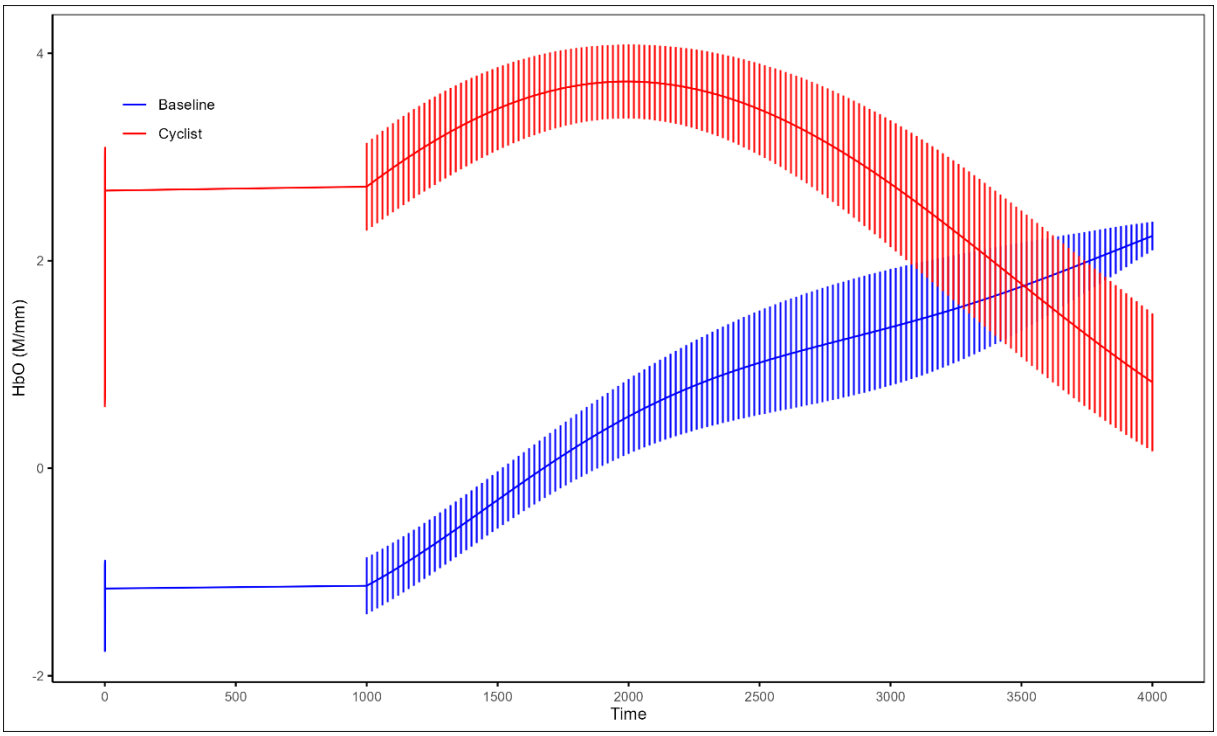

Figure A3

Comparing Event Intersection with Baseline at the Right-DLPFC

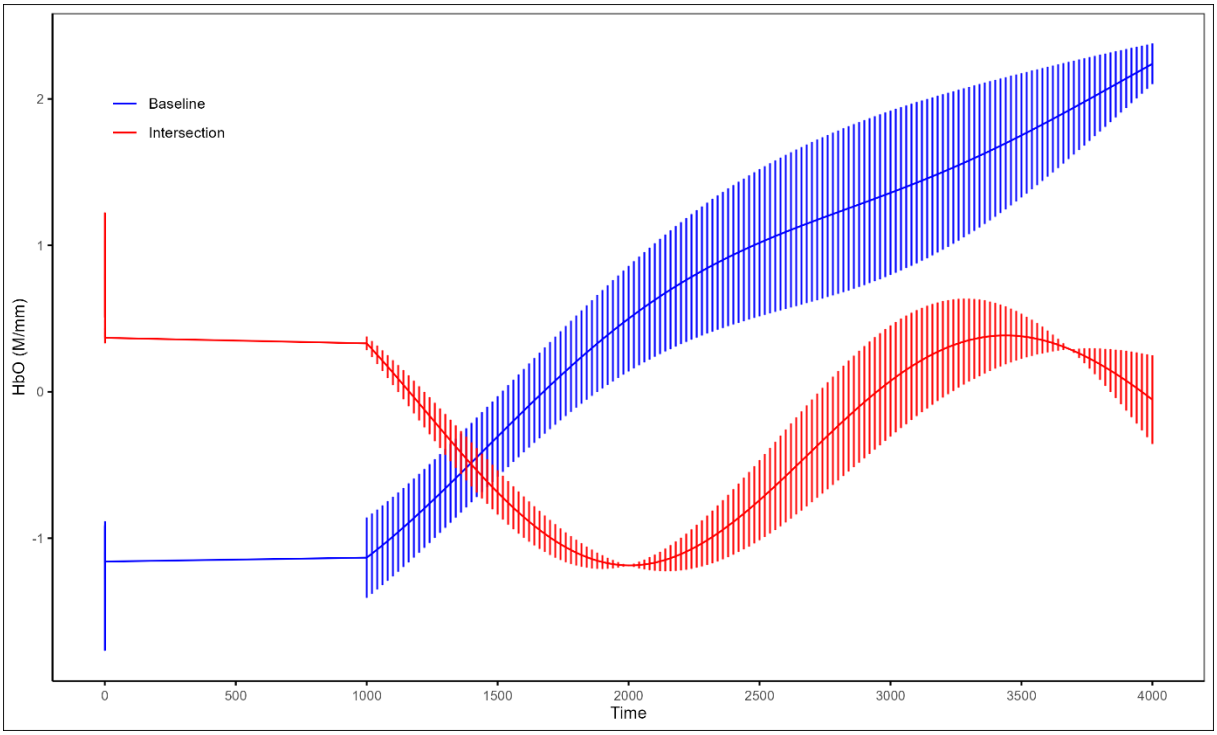

Figure A4

Comparing Event Motorized Vehicle with Baseline at the Right-DLPFC

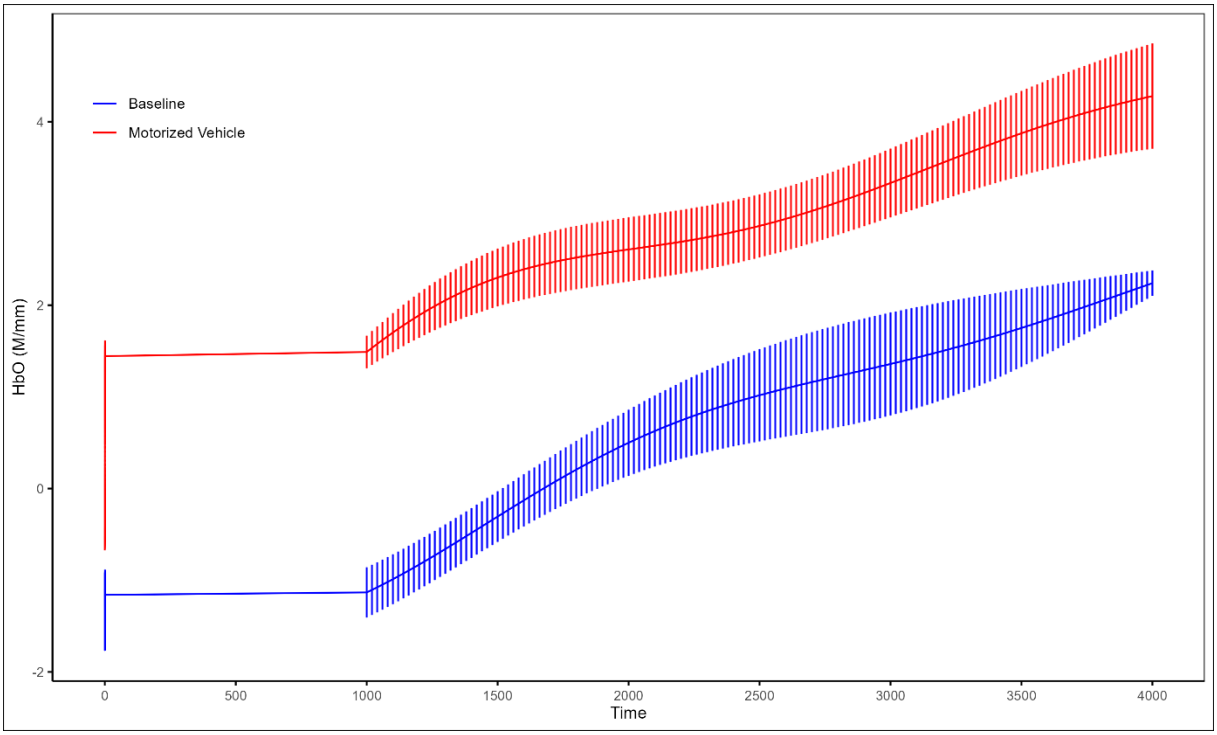

Figure A5

Comparing Event Roundabout with Baseline at the Right-DLPFC

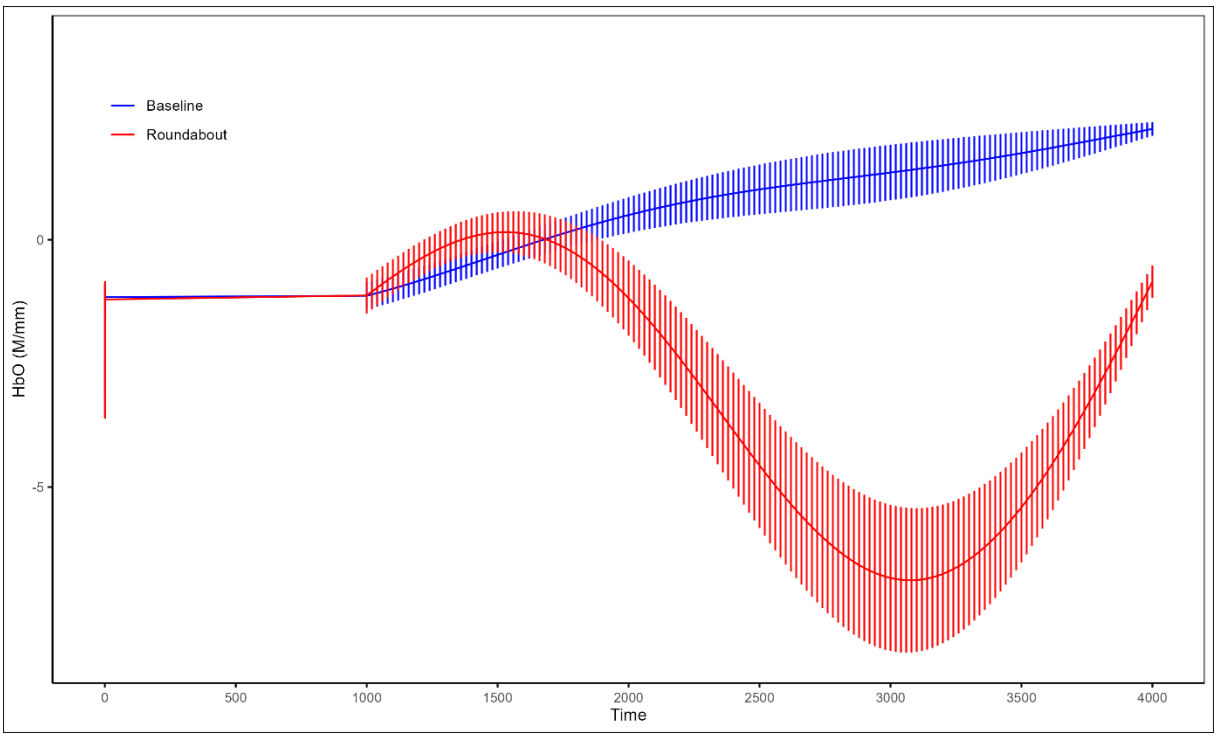

Figure A6

Comparing Event Traffic Light with Baseline at the Right-DLPFC

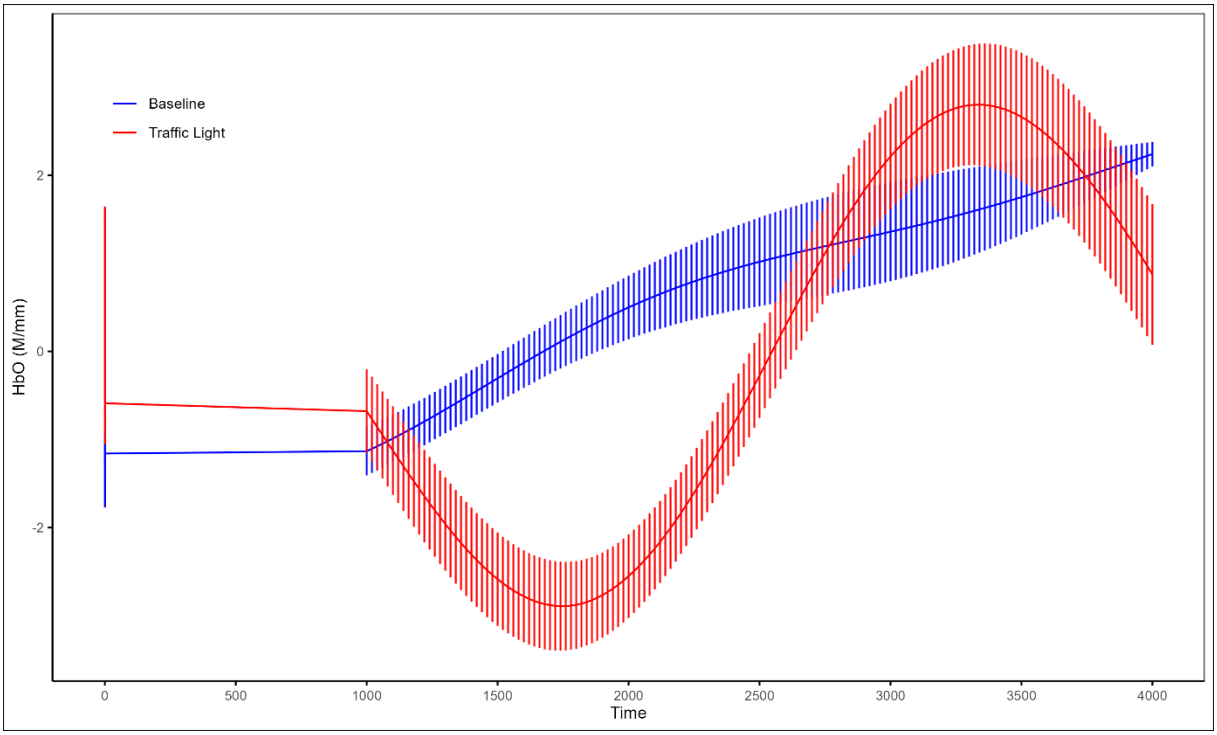

Figure A7

Comparing Event Cyclist with Baseline at the Left-DLPFC

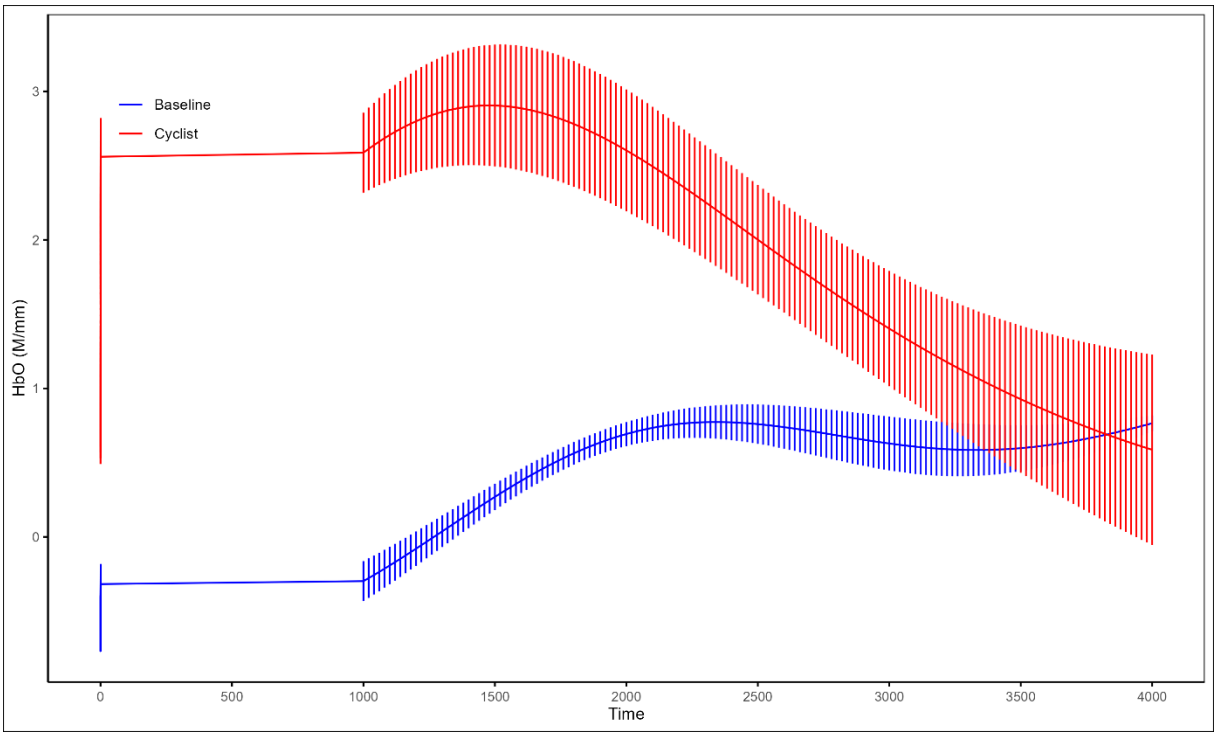

Figure A8

Comparing Event Crosswalk with Baseline at the Left-DLPFC

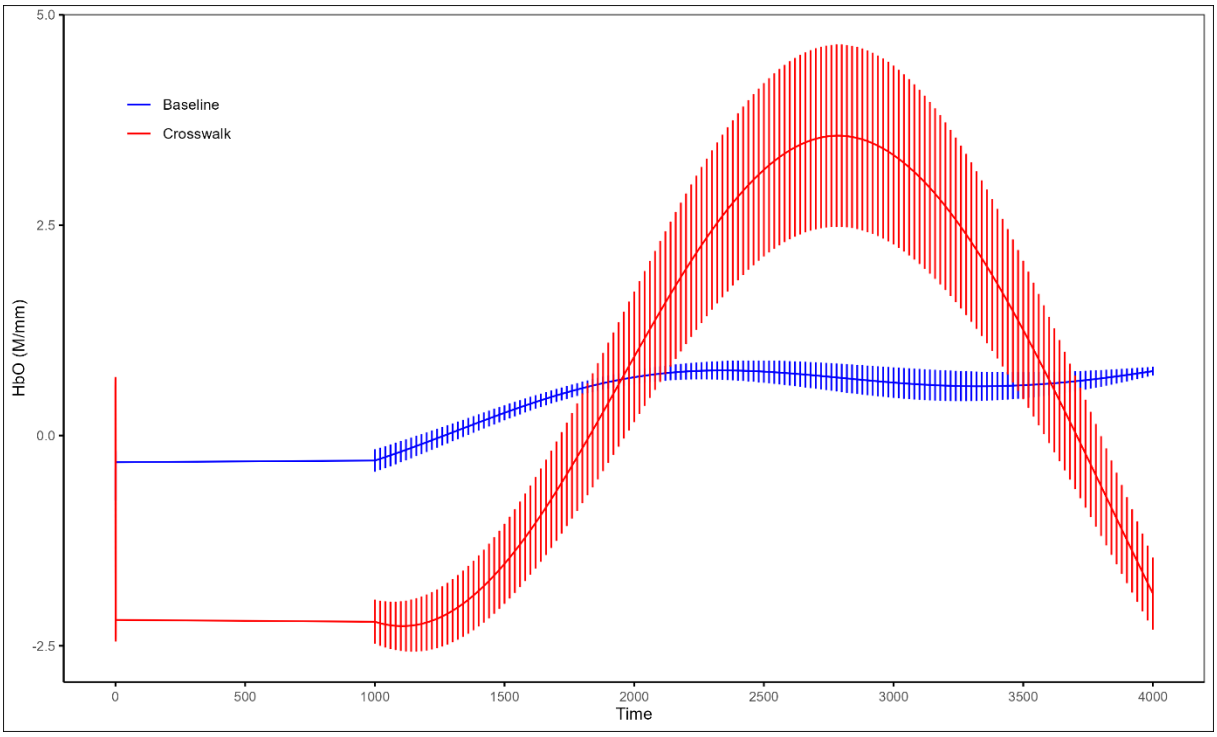

Figure A9

Comparing Event Intersection with Baseline at the Left-DLPFC

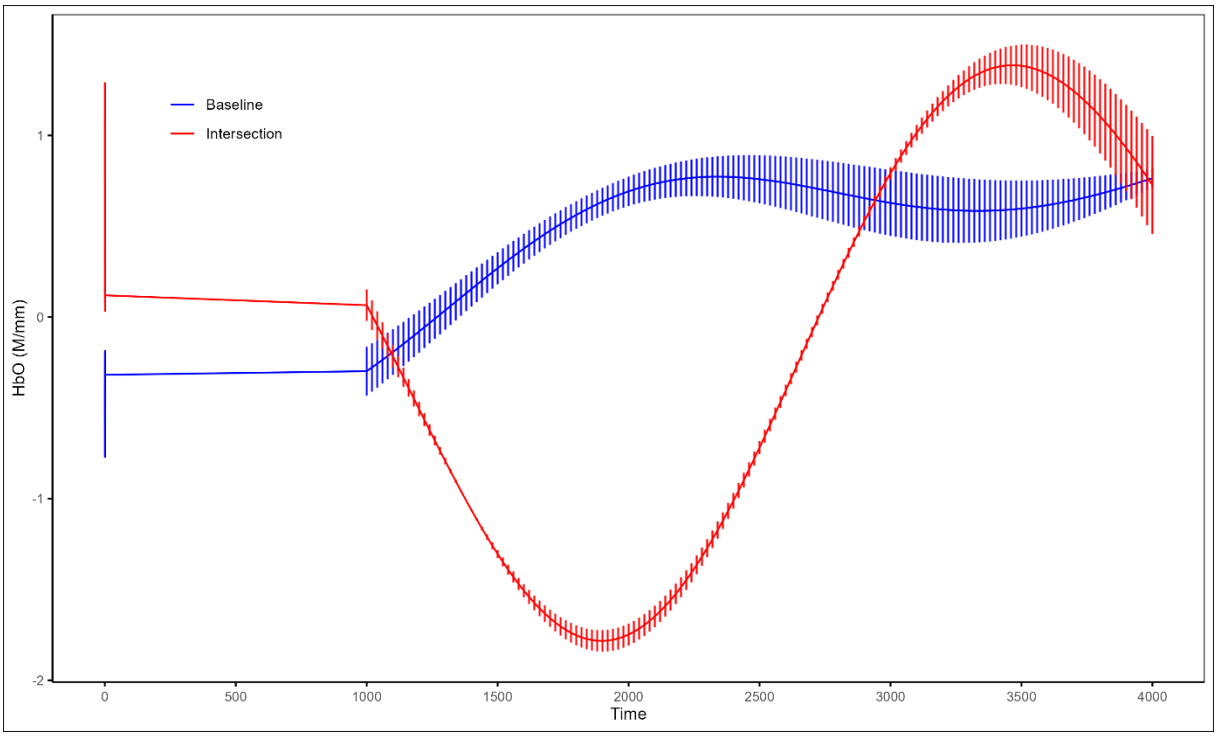

Figure A10

Comparing Event Motorized Vehicle with Baseline at the Left-DLPFC

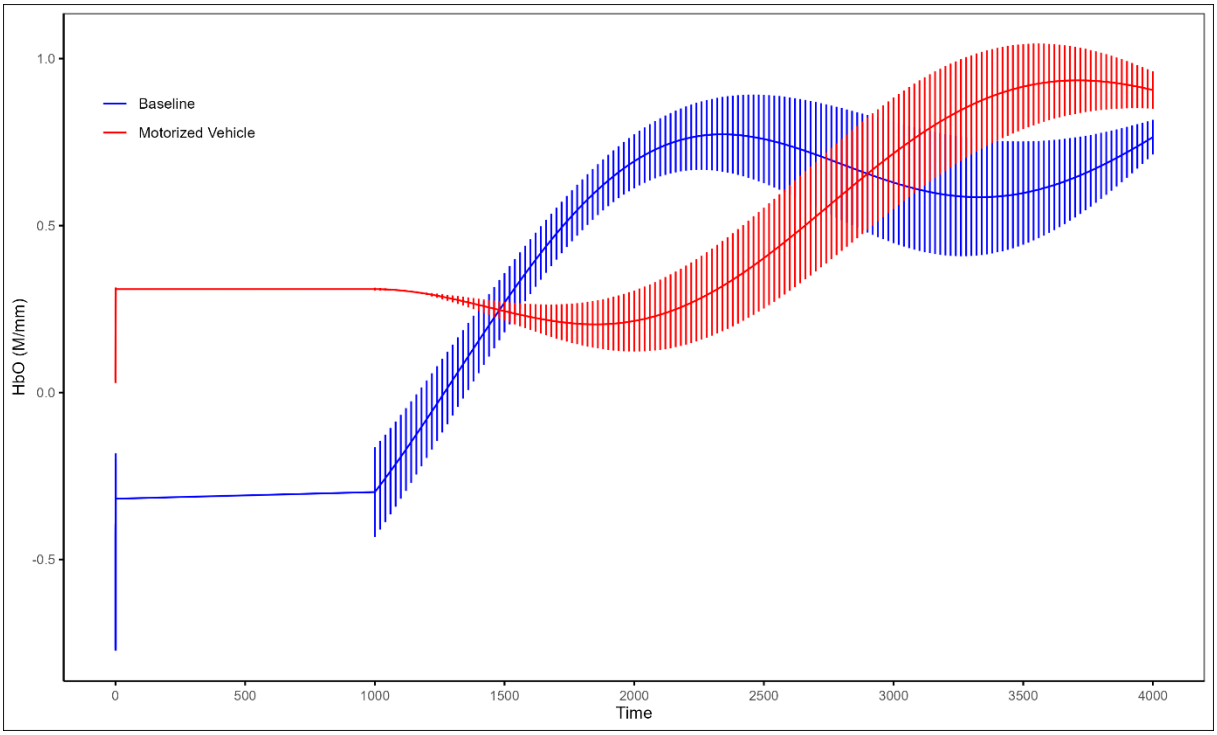

Figure A11

Comparing Event Roundabout with Baseline at the Left-DLPFC

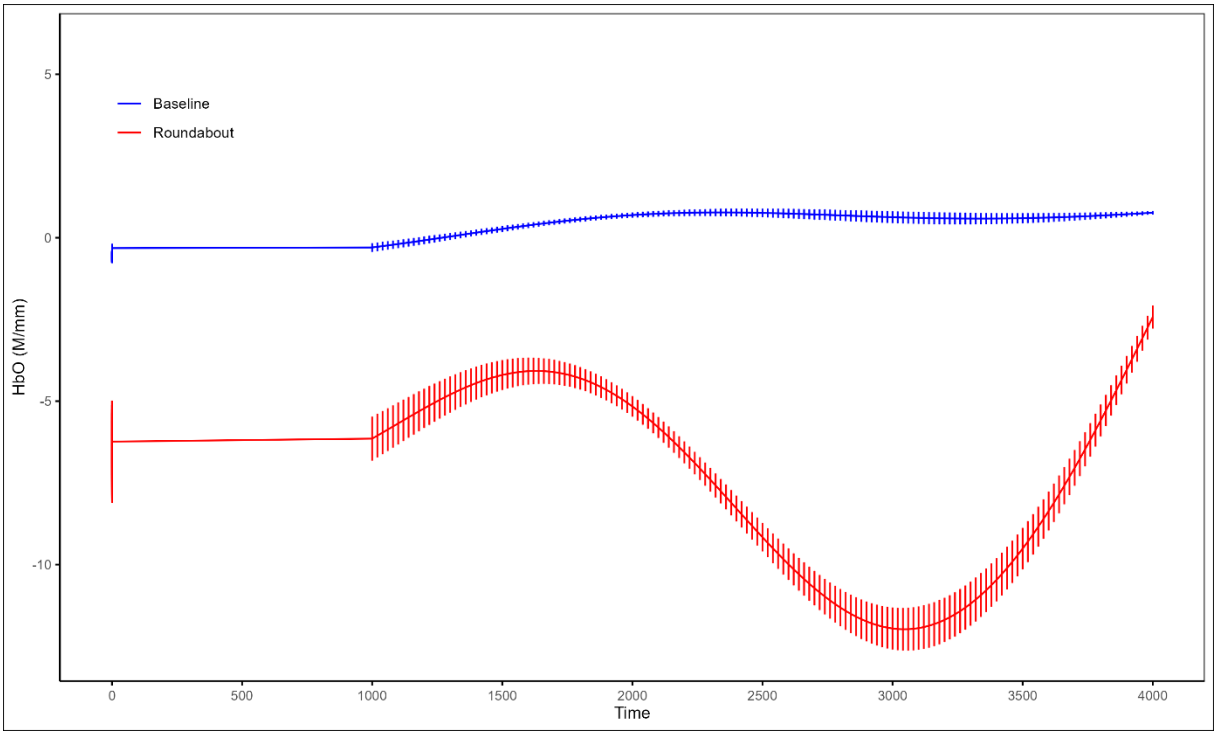

Figure A12

Comparing Event Traffic Light with Baseline at the Left-DLPFC

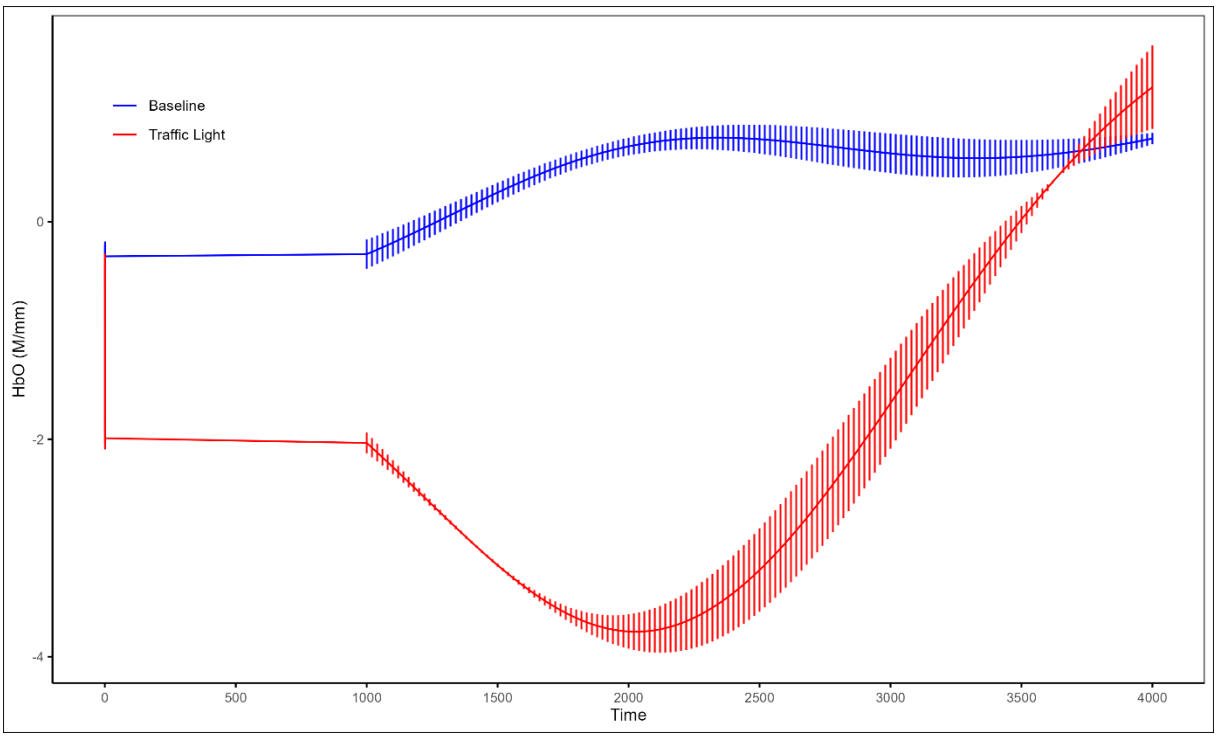

Appendix B

Channel Naming Conventions and Locations

Table B1

Table Showing Channel Naming Conventions and Locations

	Channel Name	MNI-Coordinate (x y z)	Assigned Brain Region
Channel 1	Rx1 - Tx1 (1,1)	-103,07 -59,70 34,75	OFC
Channel 2	Rx2 - Tx1 (1,2)	-77,65 -82,73 44,43	OFC
Channel 3	Rx1 - Tx2 (2,1)	-109,32 -22,60 54,85	DLPFC
Channel 4	Rx3 - Tx2 (2,3)	-86,61 -2,77 84,88	DLPFC
Channel 5	Rx1 - Tx3 (3,1)	-84,39 -46,20 74,14	OFC
Channel 6	Rx2 - Tx3 (3,2)	-58,97 -69,23 83,82	VMPFC
Channel 7	Rx3 - Tx3 (3,3)	-61,69 -26,37 104,18	DMPFC
Channel 8	Rx4 - Tx3 (3,4)	-30,57 -50,71 106,84	VMPFC
Channel 9	Rx2 - Tx4 (4,2)	-28,58 -91,20 76,87	VMPFC
Channel 10	Rx4 - Tx4 (4,4)	-0,17 -72,68 99,89	VMPFC
Channel 11	Rx6 - Tx4 (4,6)	28,07 -91,81 76,31	VMPFC
Channel 12	Rx3 - Tx5 (5,3)	-31,18 -3,80 117,85	DMPFC
Channel 13	Rx4 - Tx5 (5,4)	-0,05 -28,13 120,51	DMPFC
Channel 14	Rx5 - Tx5 (5,5)	0,06 31,50 116,40	DMPFC
Channel 15	Rx7 - Tx5 (5,7)	31,18 -4,61 117,82	DMPFC
Channel 16	Rx3 - Tx6 (6,3)	-60,95 31,32 99,58	DMPFC
Channel 17	Rx5 - Tx6 (6,5)	-29,71 66,62 98,14	DMPFC
Channel 18	Rx5 - Tx7 (7,5)	30,04 65,50 98,81	DMPFC
Channel 19	Rx7 - Tx7 (7,7)	61,15 29,39 100,22	DMPFC
Channel 20	Rx4 - Tx8 (8,4)	30,30 -51,47 106,55	VMPFC
Channel 21	Rx6 - Tx8 (8,6)	58,53 -70,60 82,97	VMPFC
Channel 22	Rx7 - Tx8 (8,7)	61,54 -27,94 103,85	DMPFC
Channel 23	Rx8 - Tx8 (8,8)	83,96 -48,29 73,26	OFC
Channel 24	Rx6 - Tx9 (9,6)	76,80 -84,31 42,76	OFC
Channel 25	Rx8 - Tx9 (9,8)	102,23 -62,00 33,05	OFC
Channel 26	Rx7 - Tx10 (10,7)	86,60 -5,03 84,79	DLPFC
Channel 27	Rx8 - Tx10 (10,8)	109,02 -25,37 54,20	DLPFC

Appendix C

Connectivity Analysis Correlation Matrices

Figure C1

Correlation Matrix of Baseline

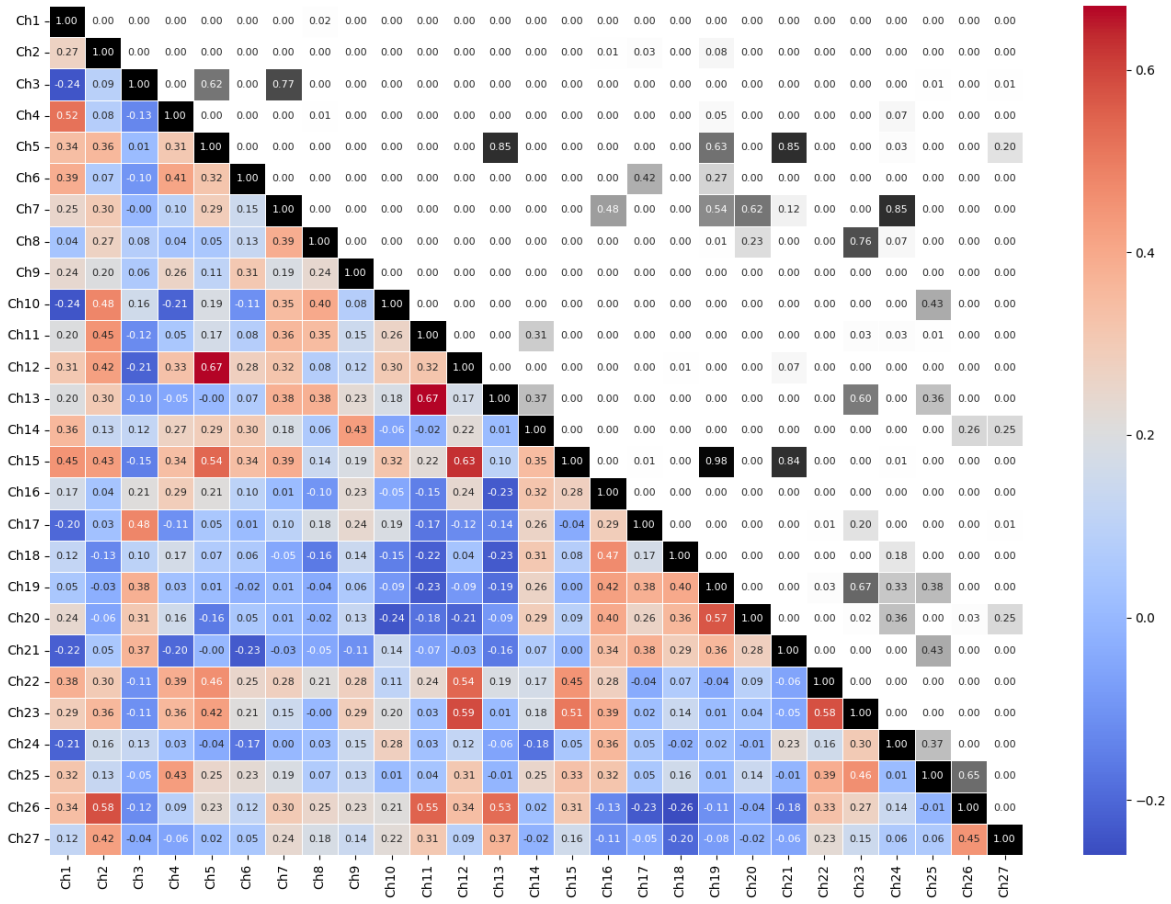

Note. The lower triangle shows the correlation coefficients. The heatmap of blue to red coloring applies to the correlation coefficients. The upper triangle shows the corresponding p-values. The higher the p-value, the darker the shading. Significant p-values (> 0.05) do not have any shading.

Figure C2

Correlation Matrix of Event Avoiding Object

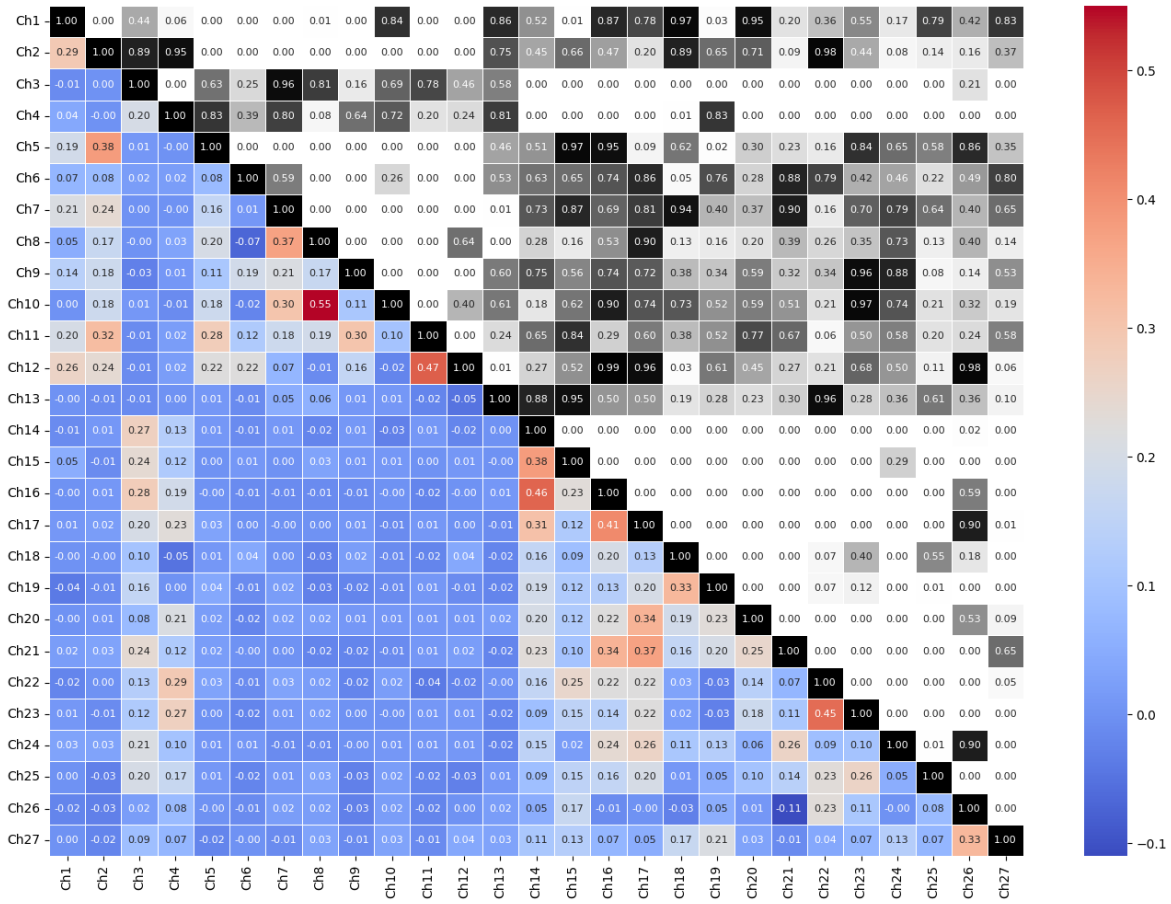

Note. The lower triangle shows the correlation coefficients. The heatmap of blue to red coloring applies to the correlation coefficients. The upper triangle shows the corresponding p-values. The higher the p-value, the darker the shading. Significant p-values (> 0.05) do not have any shading.

Figure C3

Correlation Matrix of Event Cyclist

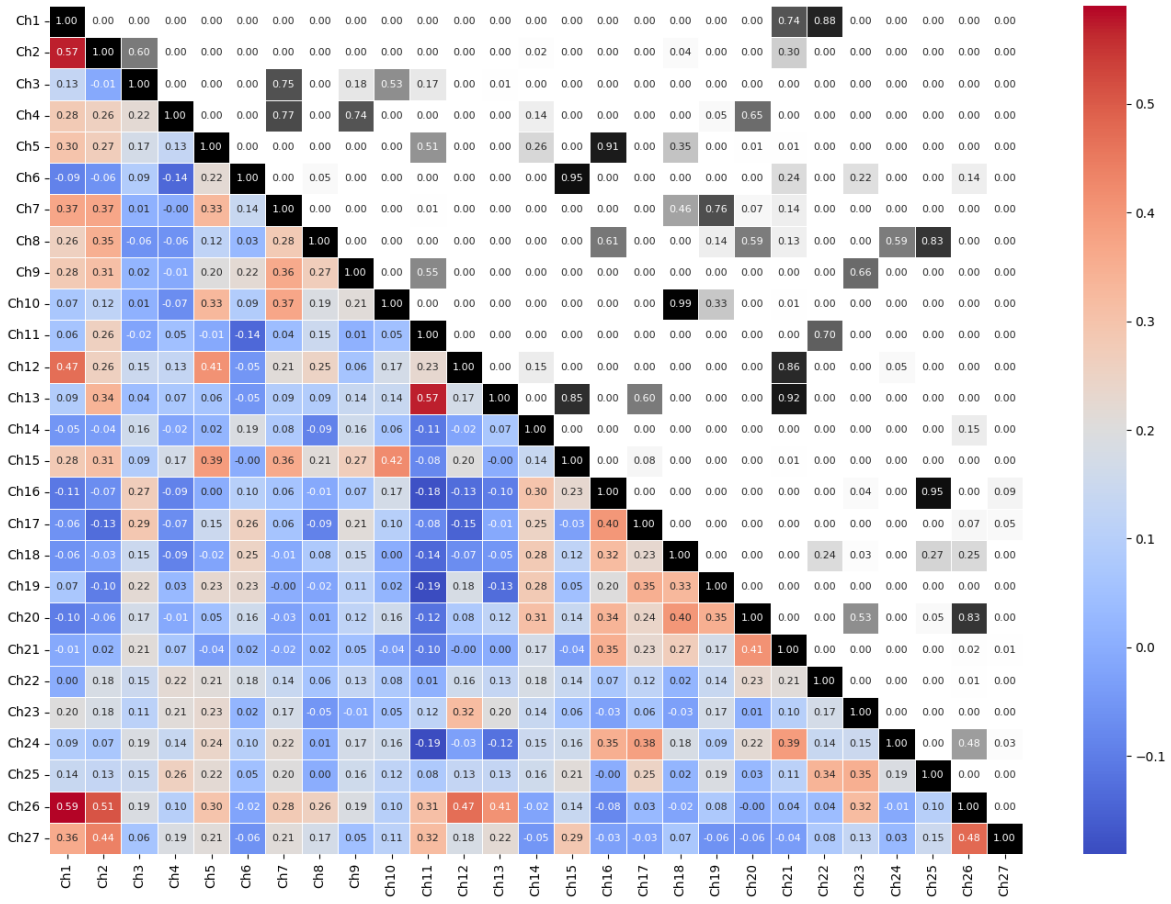

Note. The lower triangle shows the correlation coefficients. The heatmap of blue to red coloring applies to the correlation coefficients. The upper triangle shows the corresponding p-values. The higher the p-value, the darker the shading. Significant p-values (> 0.05) do not have any shading.

Figure C4

Correlation Matrix of Event Crosswalk

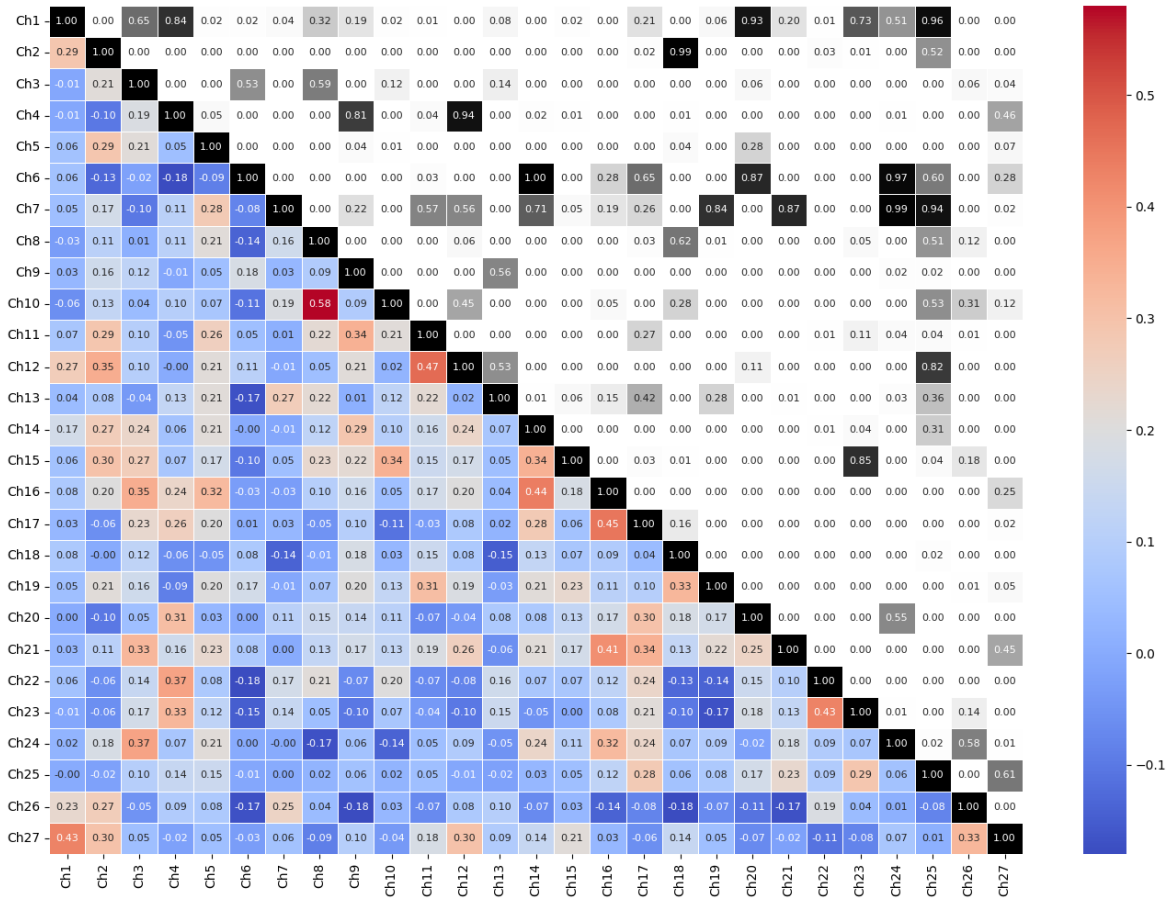

Note. The lower triangle shows the correlation coefficients. The heatmap of blue to red coloring applies to the correlation coefficients. The upper triangle shows the corresponding p-values. The higher the p-value, the darker the shading. Significant p-values (> 0.05) do not have any shading.

Figure C5

Correlation Matrix of Event Intersection

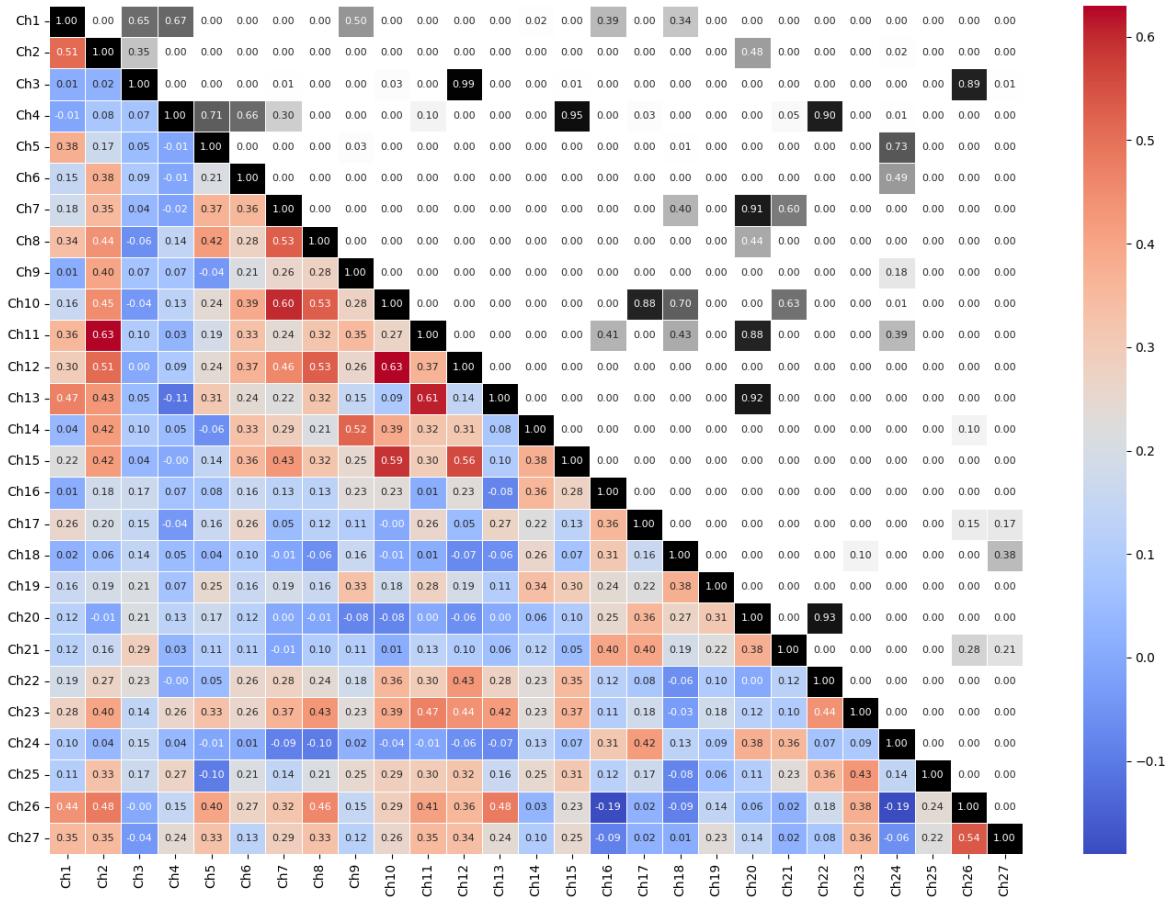

Note. The lower triangle shows the correlation coefficients. The heatmap of blue to red coloring applies to the correlation coefficients. The upper triangle shows the corresponding p-values. The higher the p-value, the darker the shading. Significant p-values (> 0.05) do not have any shading.

Figure C6

Correlation Matrix of Event Motorized Vehicle

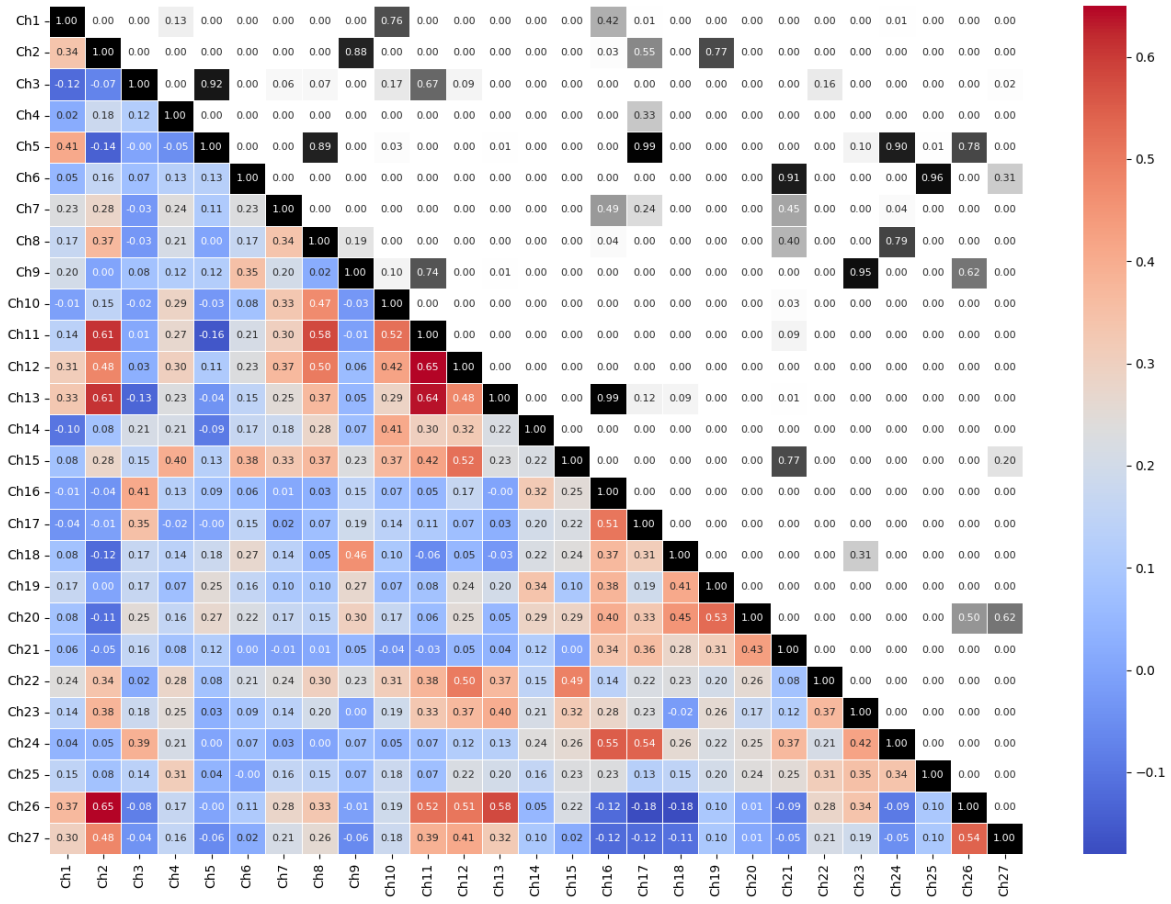

Note. The lower triangle shows the correlation coefficients. The heatmap of blue to red coloring applies to the correlation coefficients. The upper triangle shows the corresponding p-values. The higher the p-value, the darker the shading. Significant p-values (> 0.05) do not have any shading.

Figure C7

Correlation Matrix of Event Pedestrian

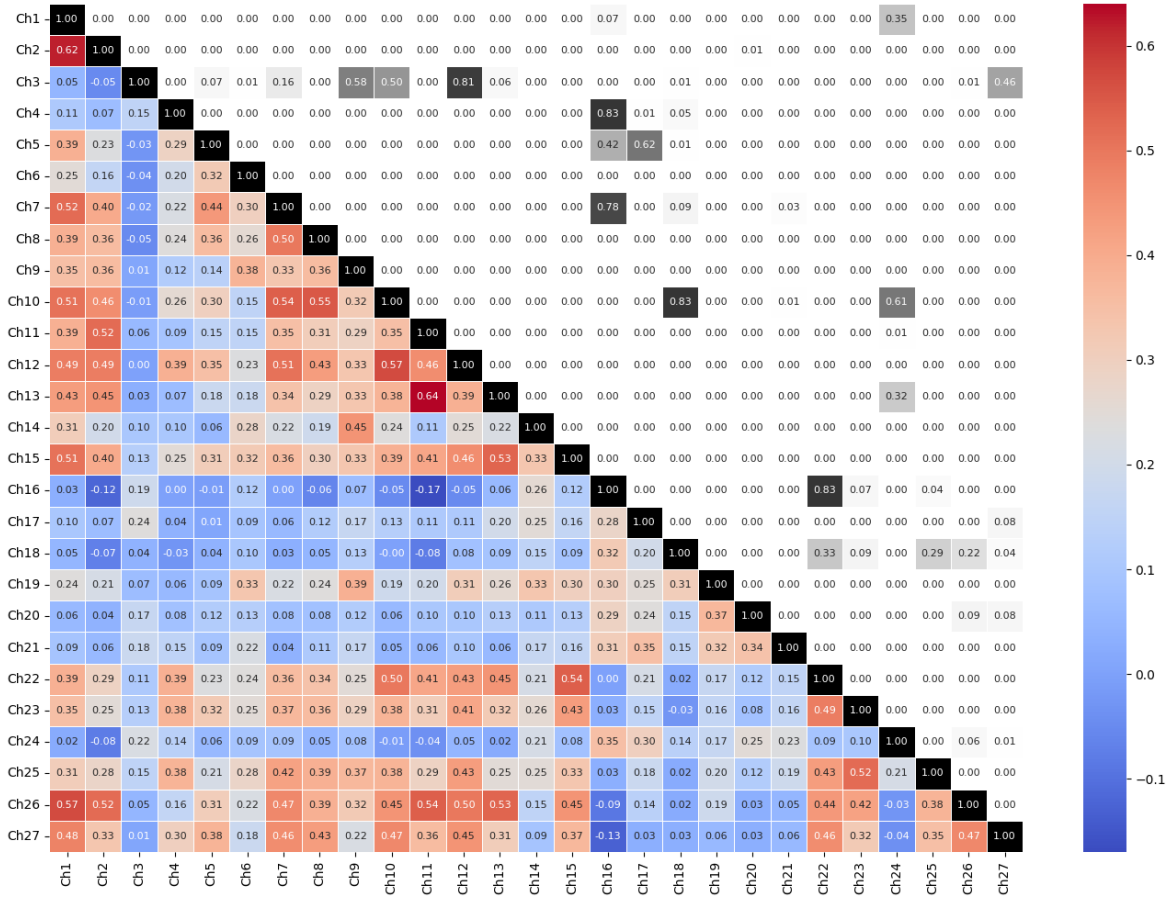

Note. The lower triangle shows the correlation coefficients. The heatmap of blue to red coloring applies to the correlation coefficients. The upper triangle shows the corresponding p-values. The higher the p-value, the darker the shading. Significant p-values (> 0.05) do not have any shading.

Figure C8

Correlation Matrix of Event Roundabout

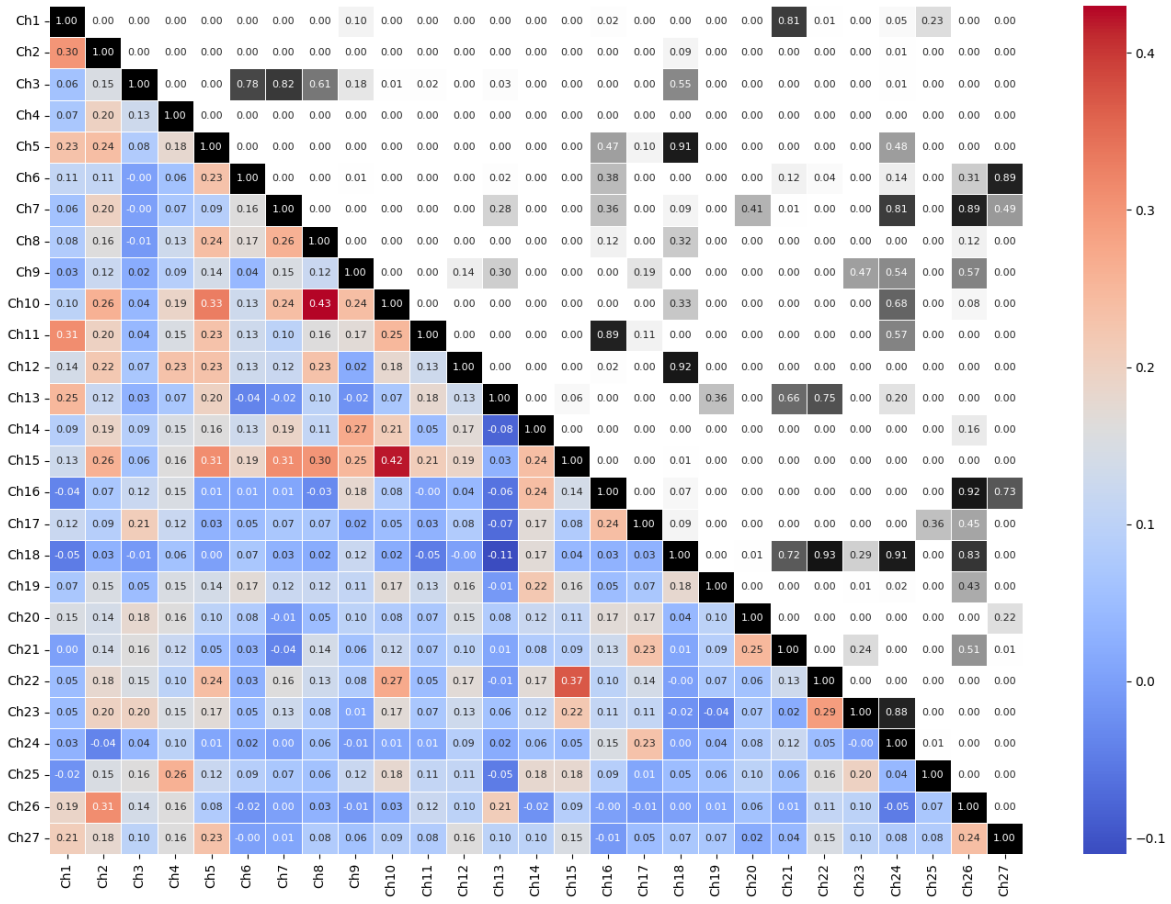

Note. The lower triangle shows the correlation coefficients. The heatmap of blue to red coloring applies to the correlation coefficients. The upper triangle shows the corresponding p-values. The higher the p-value, the darker the shading. Significant p-values (> 0.05) do not have any shading.

Figure C9

Correlation Matrix of Event Traffic Light

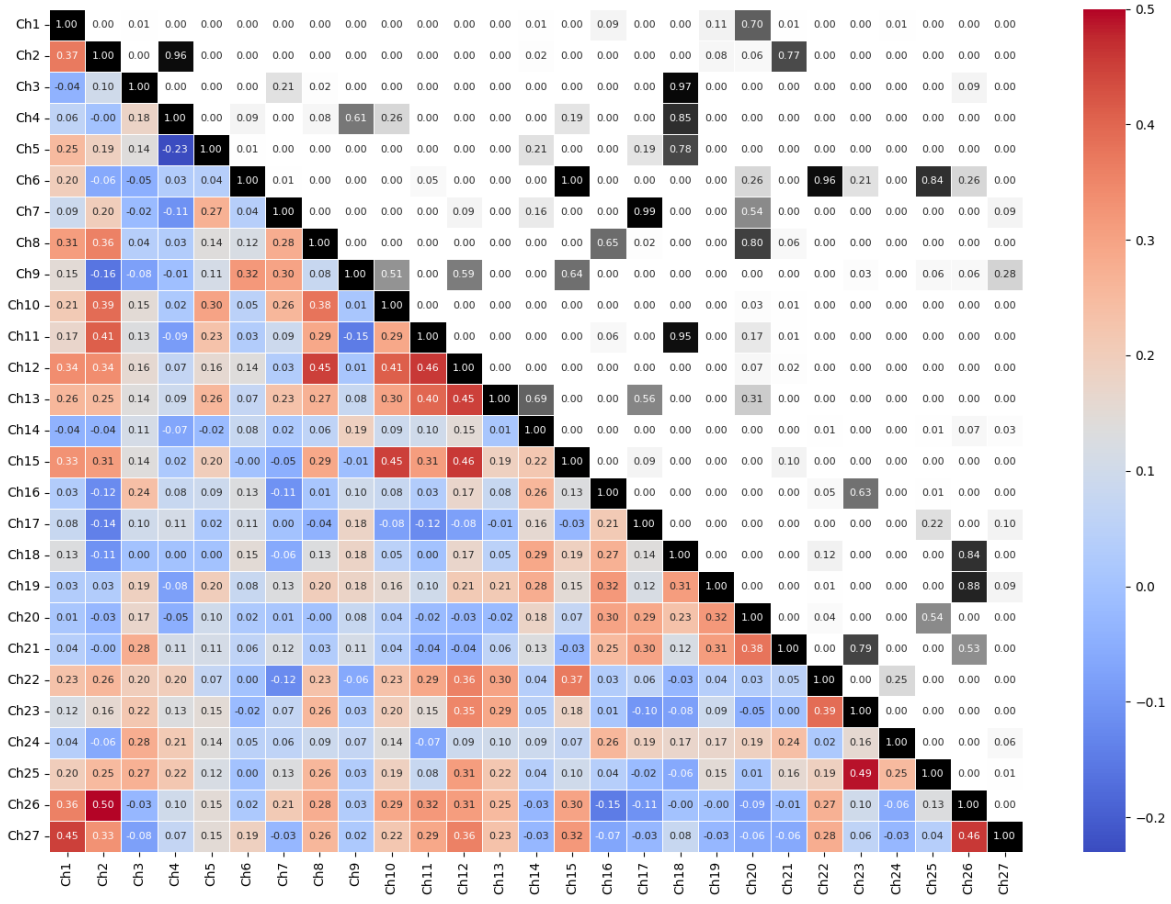

Note. The lower triangle shows the correlation coefficients. The heatmap of blue to red coloring applies to the correlation coefficients. The upper triangle shows the corresponding p-values. The higher the p-value, the darker the shading. Significant p-values (> 0.05) do not have any shading.